Chapter 4

Example Designs

The flexibility to design the QRFH for varying nominal 10 dB beamwidths through proper choice of ridge/wall profiles has made it a very attractive radio telescope feed antenna in the two years since the first QRFH was built. Its appeal is further increased because it is:

1. currently the only ultra-wideband feed that requires one single-ended 50 Ohm LNA per polarization;

2. the easiest to scale for operation in different frequency bands;

3. very stable and repeatable structurally. It can be accurately and cheaply machined from aluminum;

4. inherently low loss because of no dielectrics and relatively low current density with no thin metal surfaces.

As a result, there has been ample interest in quad-ridge horns designed at Caltech. Table 4.1 lists status of all the QRFH designs built to date in addition to those that are currently in discussion. Figure 4.1 displays this list in a more visual format.

Majority of today's cm-wave radio telescopes have f-numbers (f/D ratios) between 0.3 and 0.5 at primary, because low f-numbers yield more compact telescope designs. On the other hand, there are some notable secondary focus antennas with high f/D such as the Green Bank Telescope, the 65 meter antenna at Shanghai Astronomical Observatory, and NASA's Deep Space Network antennas[1].

In this chapter, simulated—and, where available, measured—performance of five QRFH antennas are presented. The designs are selected to demonstrate the suitability of the quad-ridge horn in telescopes with f-numbers from 0.3 to 2.5. Measured system performance of a radio telescope with one of the quad-ridge designs presented herein is also provided while predicted system performance curves are included for the remaining designs. A square QRFH design is demonstrated which is very

[1]Deep Space Network antennas are technically not radio telescopes, but they are sometimes used for radio astronomy.

Table 4.1: List of QRFH antennas delivered to telescopes around the world as well as those currently in discussion. The designs that are in bold print are presented herein.

Telescope	Primary Diam. [m]	QRFH 10 dB beamwidth [deg]	Frequency range [GHz]	Feed Diam & Length [cm]	Operated by	Status	See Section
NASA Goddard	**12**	**90**	**2-12**	**18 x 16.4**	**MIT Haystack Observatory**	**On telescope**	**4.4**
Westford	**18.3**	**140**	**2.3-14**	**14.3 x 11.9**	**MIT Haystack Observatory**	**On telescope**	**4.6**
Effelsberg	100	140	0.6-2.5	74.6 x 35	Max Planck Institute for Radio Astronomy	On telescope	
Caltech	6	150	0.6-3	72.6 x 32	Caltech	On telescope	
Japanese VLBI	**13.2**	**120**	**2.3-14**	**20 x 13.4**	**Geospatial Information Authority of Japan**	**Shipped**	**4.5**
Caltech OVRO	27	120	1-6 and 3-18	12.4 x 5.7 (3-18)	Caltech OVRO	In fabrication	
Haystack VLBI	N/A	120	2.3-14	20 x 13.4	MIT Haystack Observatory	Under test	
Shanghai VLBI	N/A	120	2.3-14	20 x 13.4	Shanghai Astronomical Observatory	Under test	
Deep Space Network	**70**	**30**	**0.5-3.5**	**230 x 401**	**NASA/JPL**	**In discussion**	**4.2**
Shanghai	65	30	4-28?	TBD	Shanghai Astronomical Observatory	In discussion	
Australian VLBI	N/A	90	2.3-14	TBD	CSIRO	In discussion	
GAVRT	**34**	**65**	**0.7-4.9**	**82 x 73.2**	**Lewis Center for Educational Research/Caltech**	**On hold**	**4.3**

Figure 4.1: A world map showing locations of the quad-ridge flared horns delivered to date (red place marks) and those that are in discussion phase (yellow place marks). The map was generated using Google Maps.

attractive for low-frequency operation due to relative ease of fabrication. Additionally, TE and TM mode coefficients at the aperture of the first three quad-ridge horns are presented.

The first section describes the antenna far-field measurement setup used for the QRFH measurements. The subsequent sections detail the five QRFH designs and are arranged in ascending order of nominal beamwidth. Target applications for these horns can be found in Table 4.1. Figure 4.2 compares profiles of the five horns which underscores the relationship between flare angle and nominal beamwidth. All results of this chapter, except measured and predicted system performance curves, are scaled such that the lowest frequency of operation, f_{lo}, of all quad-ridge horns is identical and relative bandwidths are used instead of absolute ones.

4.1 Pattern Measurement Setup

The radiation patterns of the quad-ridge horns were measured using a far-field pattern measurement setup on the roof of the electrical engineering building at California Institute of Technology. Figure 4.3 displays a photo and the block diagram of the far-field range. Obstacles on the roof limit the accuracy of the patterns to the -25 dB level; however, this is sufficient to determine the main beam, the first side lobes and performance in a reflector system.

Both co- and cross-polarized radiation patterns are measured in three azimuthal planes, namely ϕ = 0, 45, and 90 degrees, for θ = [-180, 180] degrees with one degree steps in the main beam.

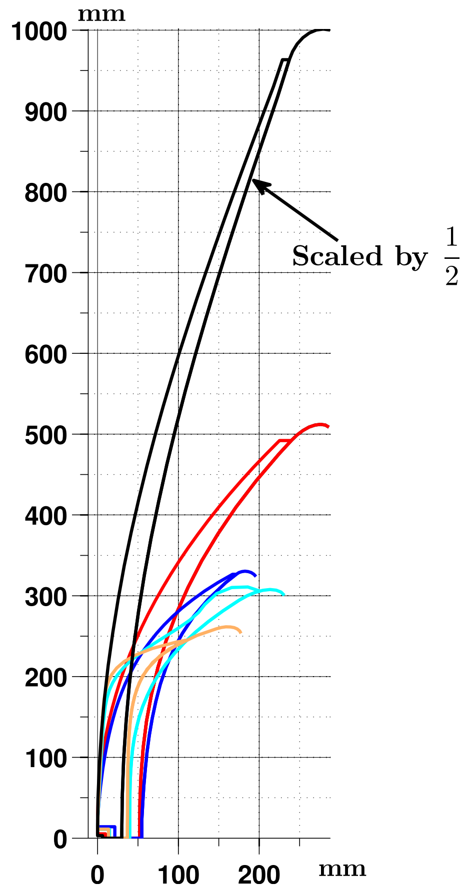

Figure 4.2: Profiles of the very high (black), high (red), medium (blue), low (cyan), and very low (orange) gain quad-ridge designs. All profiles are scaled such that their lowest frequency of operation f_{lo} is 1 GHz. Dimensions are in millimeters

(a)

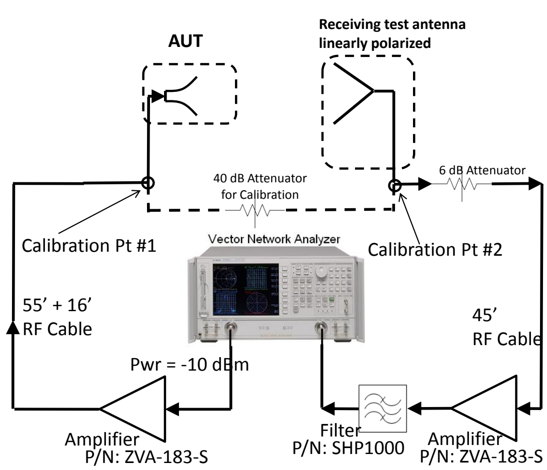

(b)

Figure 4.3: (a) Photo and (b) block diagram of the pattern measurement setup on the roof of Moore Laboratory at California Institute of Technology.

The far-field range is designed to work between 1 and 18 GHz. It is limited at the low end by very strong RFI as a result of which a high-pass filter with 1 GHz cutoff frequency is used for most of the measurements presented here. Maximum frequency of the receiving antenna, a broadband log-periodic dipole, is 18 GHz and determines the upper frequency of the pattern range.

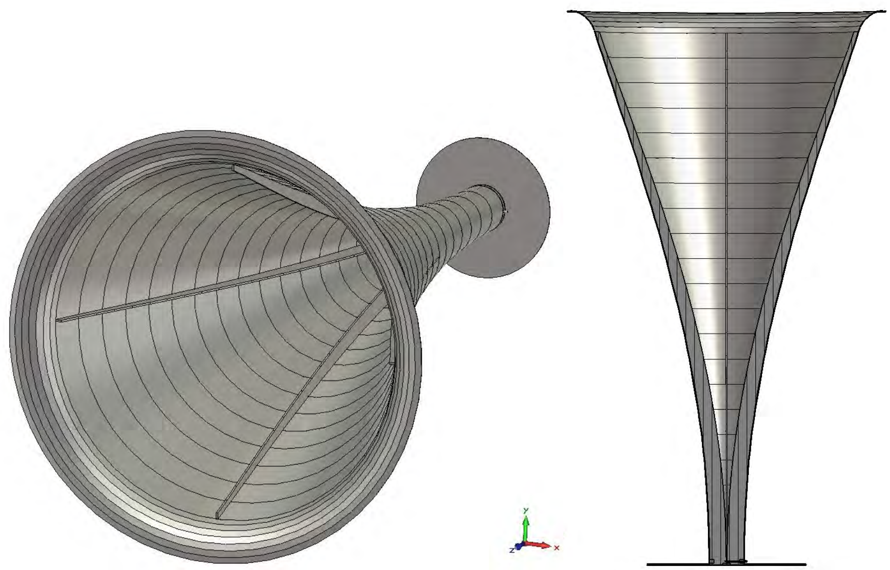

Figure 4.4: Three-dimensional CAD drawings of the very high gain quad-ridge horn. Feed diameter is 230 cm ($3.83\lambda_{lo}$) and length is 400.5 cm ($6.68\lambda_{lo}$) with $f_{lo} = 0.5$ GHz

4.2 Very-High Gain QRFH

Of the quad-ridge horns presented herein, this QRFH has undergone the least amount of optimization mainly because the interest in such high gain, wideband horns has been considerably less in the radio astronomy community. However, as this design and the next show, the high-gain quad-ridge designs achieve 7:1 bandwidths and perform as well as, if not better than, the lower gain designs.

4.2.1 Application

The intended application of the very high gain quad-ridge horn is as a low-frequency feed, primarily for pulsar timing experiments, on the 70 meter DSS-14 antenna located at the Goldstone Deep Space Communication Complex near Barstow, California. DSS-14 comprises of two mirrors in Cassegrain configuration and the feed antennas are located at the vertex of the primary mirror. The full subtended angle to the secondary reflector is 32 degrees ($f/D = 1.78$).

4.2.2 Simulations

The nominal 10 dB beamwidth of this feed is 30-32 degrees which yields somewhat high edge taper; however, the horn size becomes prohibitively large for narrower beamwidths. The ridge and sidewall tapers use the asymmetric sine-squared profile of Table 3.1. This is the largest quad-ridge horn designed as part of this research with an aperture diameter of approximately $3.3\lambda_{lo}$ and length of around $6.4\lambda_{lo}$. The flare angle is 19 degrees.

The simulated reflection coefficients of both polarizations are plotted in Figure 4.5 along with

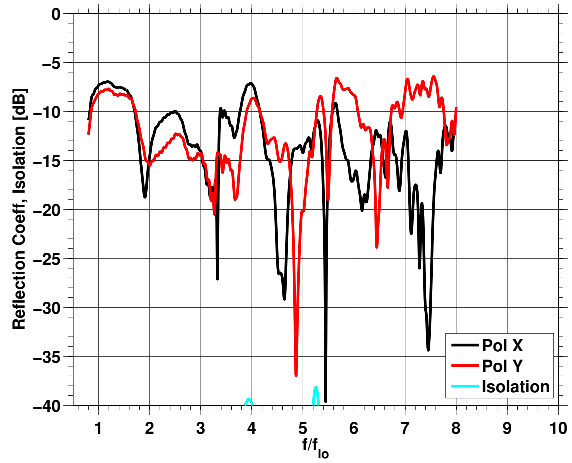

Figure 4.5: Simulated scattering parameters of the very high gain QRFH

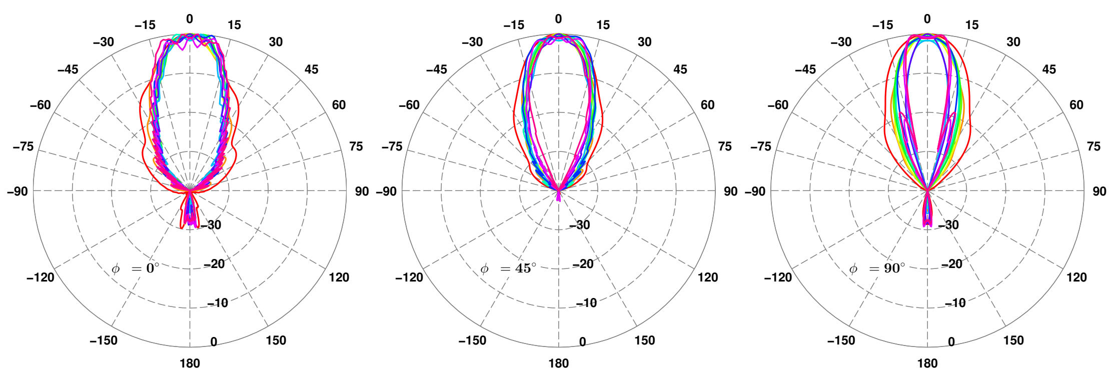

(a)

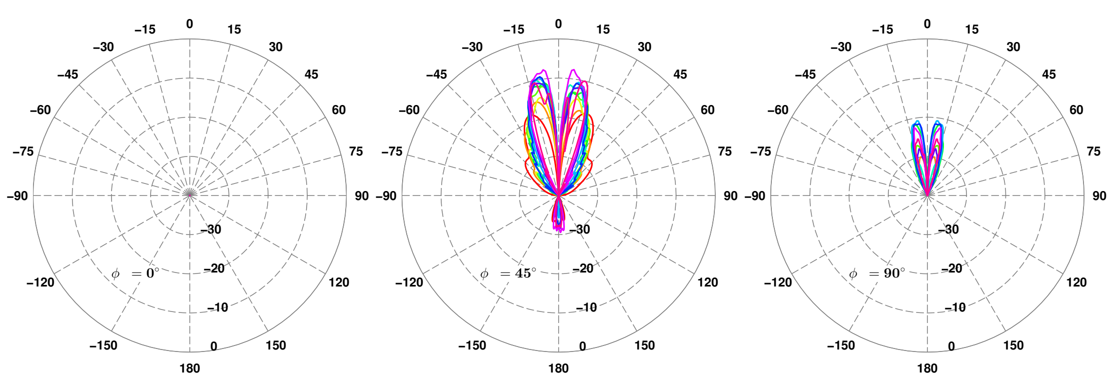

(b)

Figure 4.6: Simulated (a) co-polarized, (b) cross-polarized (Ludwig 3rd definition) radiation patterns of the very high gain QRFH in $\phi = 0°$, $45°$, $90°$ azimuthal planes over the frequency range $f/f_{lo} =$ [1, 7]

isolation between the two polarizations. The match needs improvement; it is the worst among the QRFH designs presented herein which is mainly due to insufficient optimization.

Figure 4.6 presents polar plots of the co- and cross-polarized radiation patterns (Ludwig's 3rd definition [33]) in the $\phi = 0^\circ\,(E)$, $45^\circ\,(D)$, $90^\circ\,(H)$ planes. The three-dimensional, total far-field patterns are displayed in Figure 4.7. The 10 dB beamwidths in the E- and D-planes are approximately 30 degrees, while the H-plane beamwidth varies between 40 and 20 degrees. There are no visible sidelobes, backlobes are at least 30 dB down from boresight, and the beam is well-formed and shows no splitting over 7:1 frequency range. The cross-polarization in the diagonal plane is better than -10 dB over most of the band, and peaks to about -9 dB over very narrow frequency range.

Intensity plots (function of both phase and magnitude) of x-directed electric field, E_x, in the horn as a function of frequency are presented in Figure 4.8. They reveal that the electric field is more tightly coupled to the ridges all the way up to the aperture for lower frequencies. On the other hand, this coupling becomes looser at higher frequencies. Qualitatively, this could be thought of as radiation beginning further in the horn at higher frequencies. The fields seem to "break up" around 6-7 f_{lo} showing considerable intensity near the ridges, which may be because of reflections due to unwanted mode coupling.

4.2.3 Aperture mode content

The mode coefficients at the aperture of the very high gain QRFH are calculated using the method described in Appendix 3.5. The modes required to generate the desired radiation patterns are also calculated using the same approach. Figure 4.9 presents these normalized mode coefficients where only the first four modes needed for the desired radiation patterns are plotted.

These curves show that the simulated mode content at the aperture comes fairly close to the desired mode distribution; however, better mode control is needed, especially for TM modes. Furthermore, there is fine structure in the simulated coefficients in the middle as well as the upper end of the frequency range. This is believed to be in part due to the limited optimization this design has undergone. The field "break up" around 6–7 f_{lo}, mentioned in the previous subsection, seems to be correlated strongly with decrease in TE_{11} and TM_{11} coefficients while TE_{12} and TE_{13} coefficients become more prominent.

Another observation from these plots is the absence of even-order azimuthal modes, which is an important result that suggests that ridges do not significantly alter the mode conversion expected from a smooth-walled horn with the identical profile. In particular, it was shown in [54] that horn diameter variations can only cause coupling between modes of same azimuthal order.

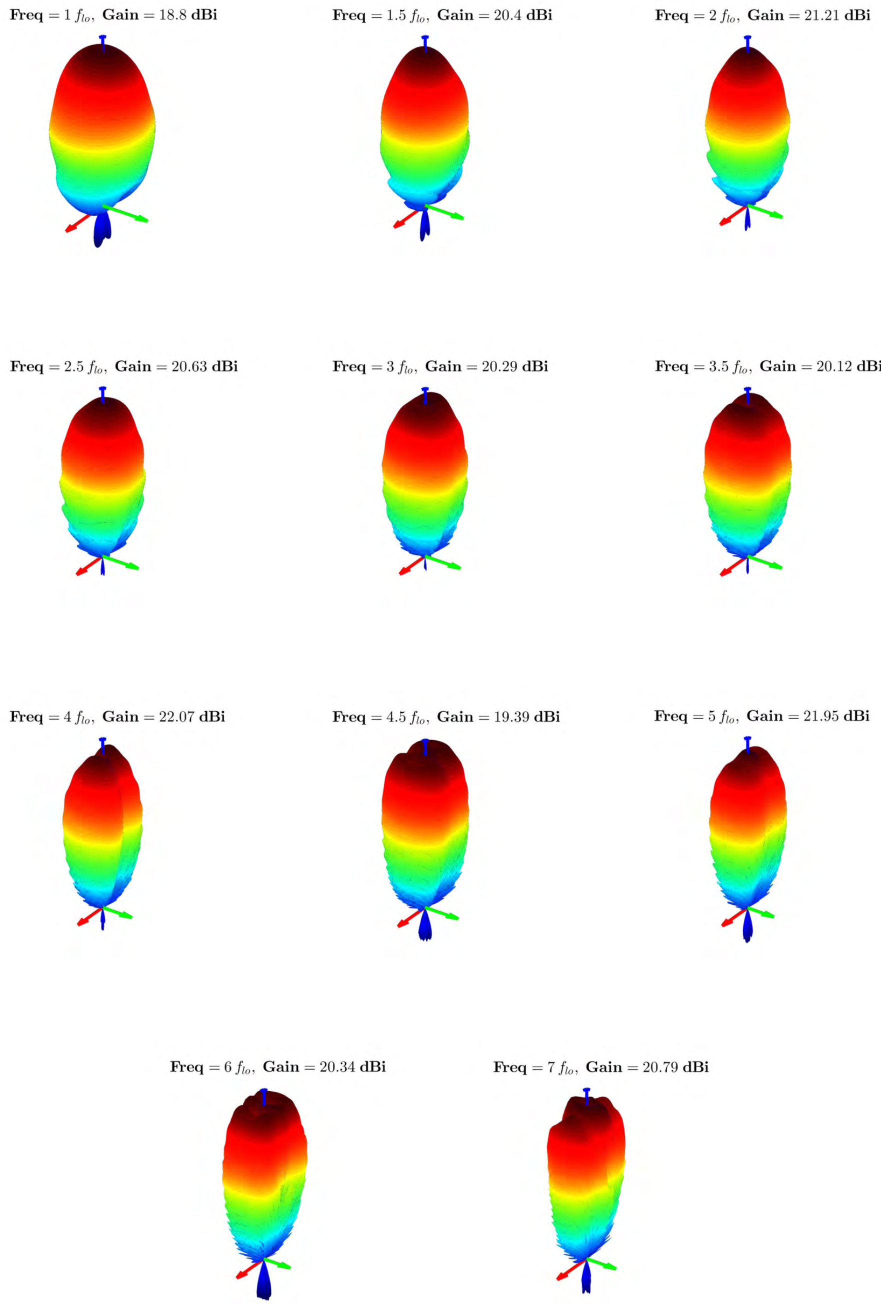

Figure 4.7: Three dimensional radiation patterns of the very high gain QRFH.

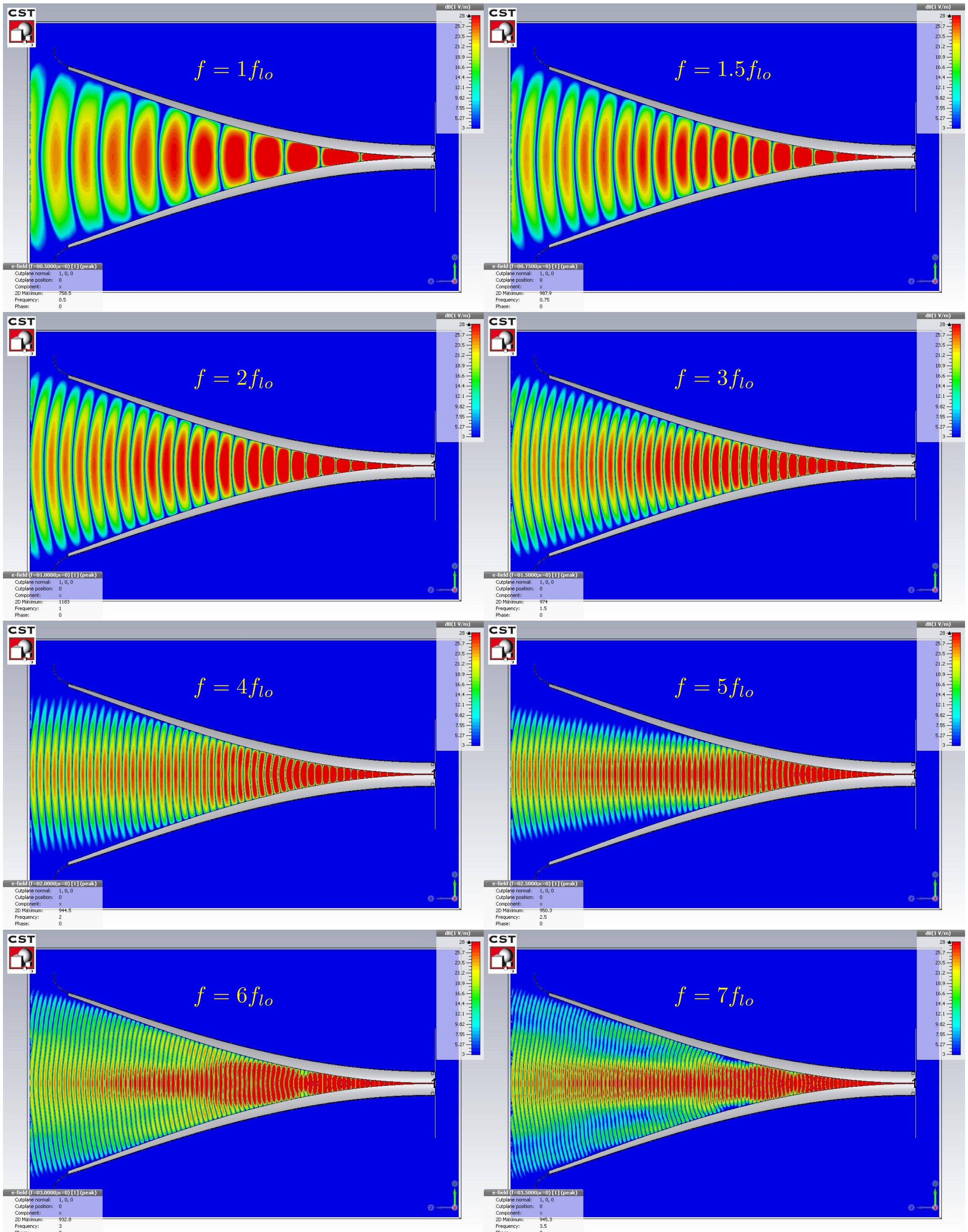

Figure 4.8: Intensity plots of E_x on the $x = 0$ plane in the very high gain quad-ridge horn which is excited in the x-polarization.

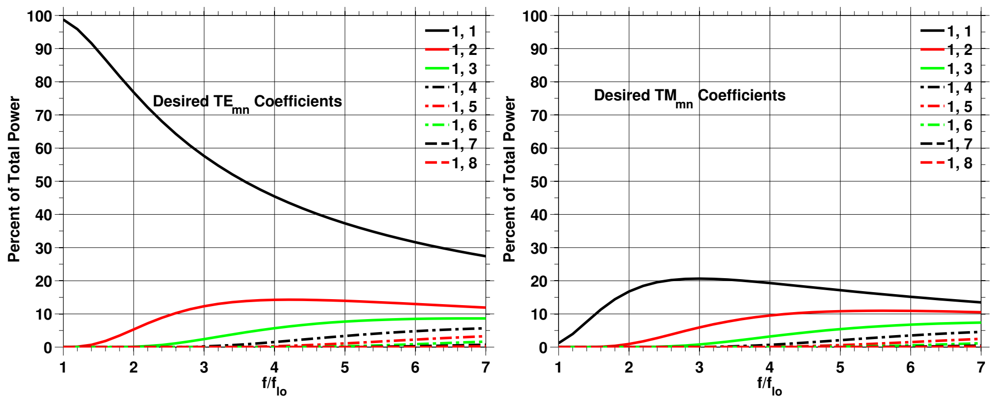

(a)

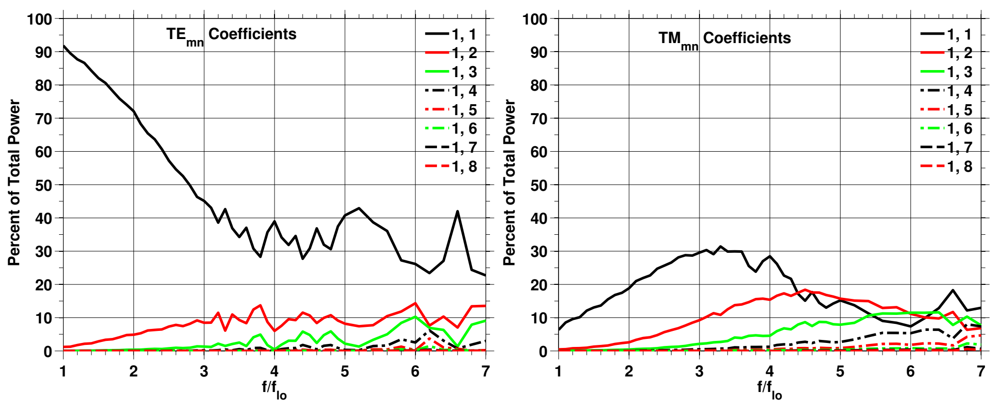

(b)

Figure 4.9: Normalized mode coefficients (a) required to achieve the desired radiation pattern, (b) at the aperture of the very high gain QRFH calculated using the simulated patterns. While all the modes present in the horn are not plotted, the modes plotted account for well more than 99% of the total power.

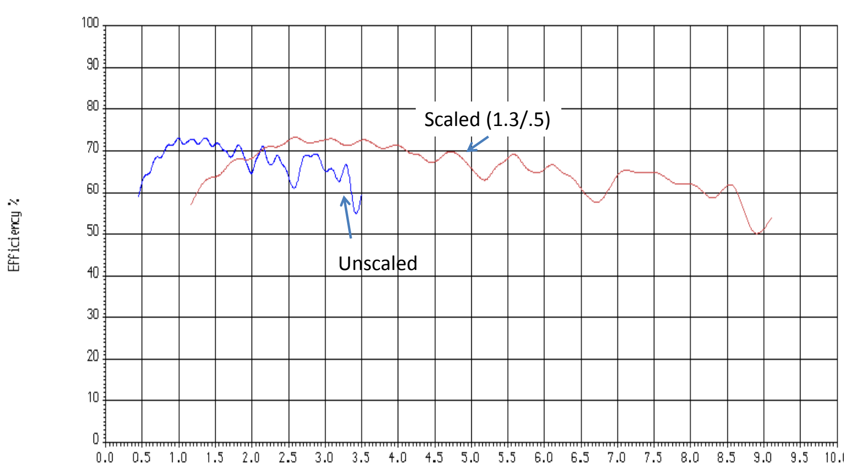

Figure 4.10: Predicted aperture efficiency of the DSS-14 70-meter antenna with the very high gain QRFH as the feed antenna. The efficiency is calculated using physical optics and losses due to RMS surface error, blockage, struts, etc., are ignored.

4.2.4 Predicted system performance

This QRFH was initially designed to cover 0.5 to 3.5 GHz. The PO aperture efficiency of the DSS-14 over this frequency range with the QRFH at the secondary focus appears in Figure 4.10 in blue which is computed with simulated patterns. It is seen that the average efficiency is $> 65\%$ and the efficiency stays above 55% throughout the band. Recently, there has also been interest at a higher frequency version of this horn on the DSS-14, namely f_{lo} of 1.3 GHz. The predicted aperture efficiency of this version is also plotted in the same figure and is slightly lower, but still maintains an average of $\sim$65%. These results suggest that both horns attain 7:1 frequency bandwidth, at least according to simulations.

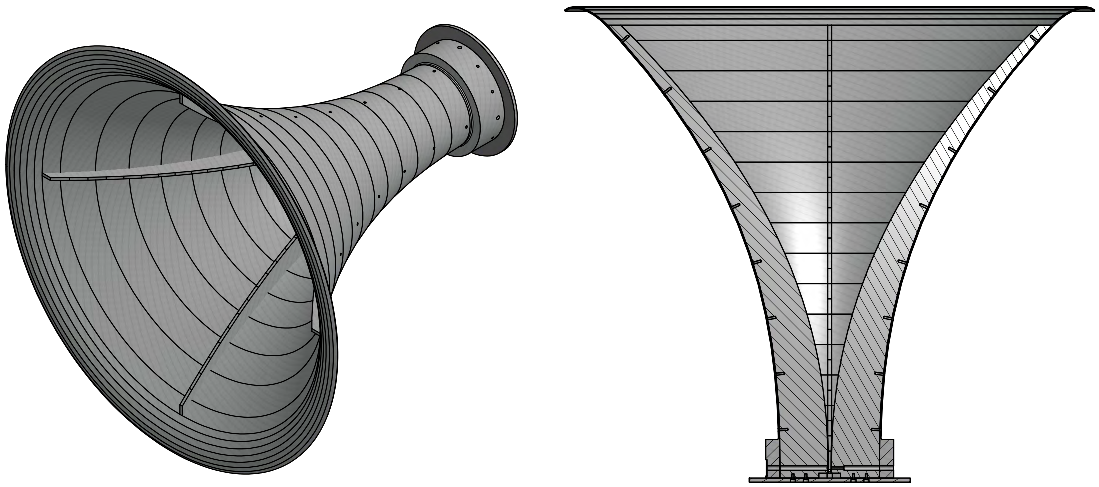

Figure 4.11: Three-dimensional CAD drawings of the high-gain quad-ridge horn. Feed diameter is 82 cm ($1.9\lambda_{lo}$) and length is 73.2 cm ($1.7\lambda_{lo}$) with $f_{lo} = 0.7$ GHz

4.3 High-Gain QRFH

4.3.1 Application

This QRFH was designed to be used as the low-frequency feed of the Goldstone Apple Valley Radio Telescope (GAVRT) [5] for wide bandwidth pulsar timing experiments. The reflector antenna of this telescope is the 34 meter DSS-28 located at the Goldstone Deep Space Communication Complex near Barstow, California. DSS-28 was initially designed for high-power transmission employing two mirrors in Cassegrain configuration and a beam-waveguide feed system [55]. The antenna was then retrofitted with a tertiary paraboloid mirror at the vertex of the dish which enabled focusing of the beam onto a feed mounted on the surface and near the vertex of the dish antenna. The full subtended angle to the tertiary mirror is 81.2 degrees, but due to the unusual optics the telescope aperture efficiency increases with increased edge taper at the tertiary reflector.

4.3.2 Simulations

The nominal 10 dB beamwidth of the quad-ridge horn is selected 65 degrees due to size restrictions near the vertex of the reflector as narrower beamwidths necessitate longer horns with wider apertures (see Figure 4.2). Both the ridge and sidewall tapers of the final design, shown in Figure 4.11, employ the x^p profile. The aperture diameter is $1.69\lambda_{lo}$ and the ridge profile length is $1.64\lambda_{lo}$. The flare angle is approximately 45 degrees.

Figure 4.12 presents the simulated S-parameters of this quad-ridge horn. The simulated reflection coefficient is better than 10 dB across the 7:1 frequency band and better than 15 dB over much of this range. Figure 4.13 displays two-dimensional cuts of the co- and cross-polarized (Ludwig's 3rd

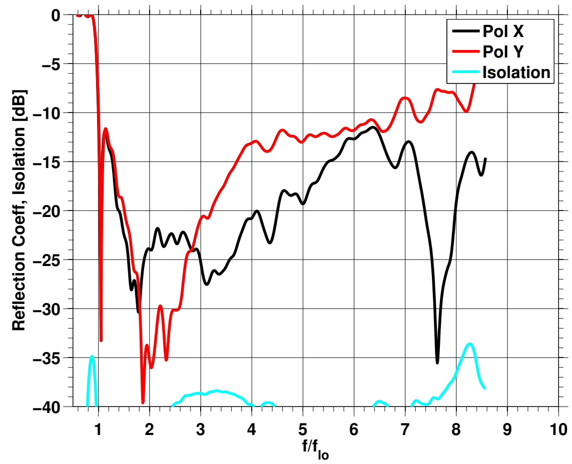

Figure 4.12: Simulated scattering parameters of the high-gain QRFH

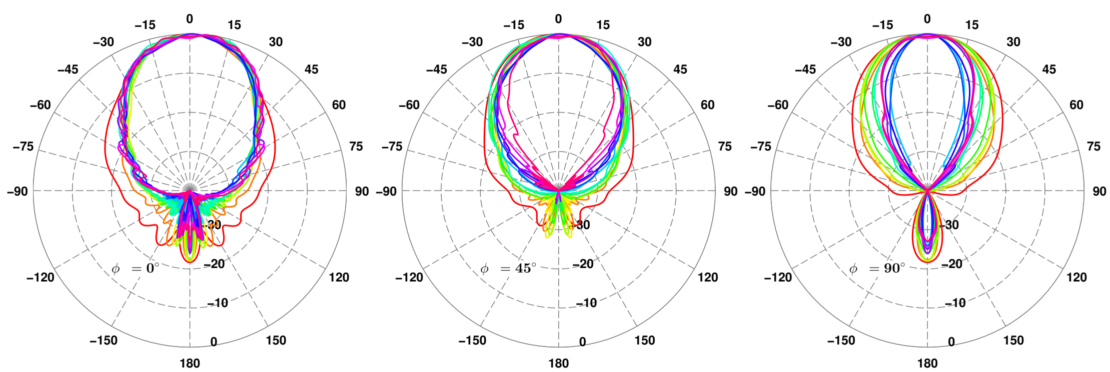

(a)

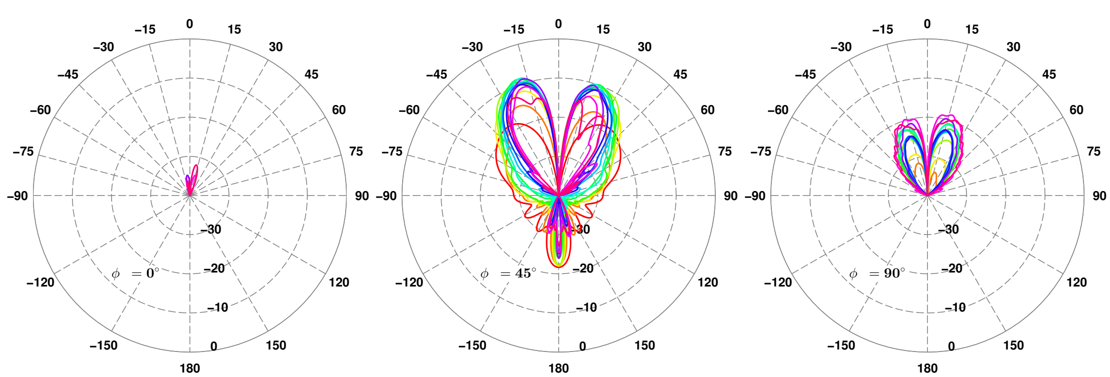

(b)

Figure 4.13: Simulated (a) co-polarized, (b) cross-polarized (Ludwig 3rd definition) radiation patterns of the high-gain QRFH in $\phi = 0°, 45°, 90°$ azimuthal planes over the frequency range $f/f_{lo} = [1,\ 7]$

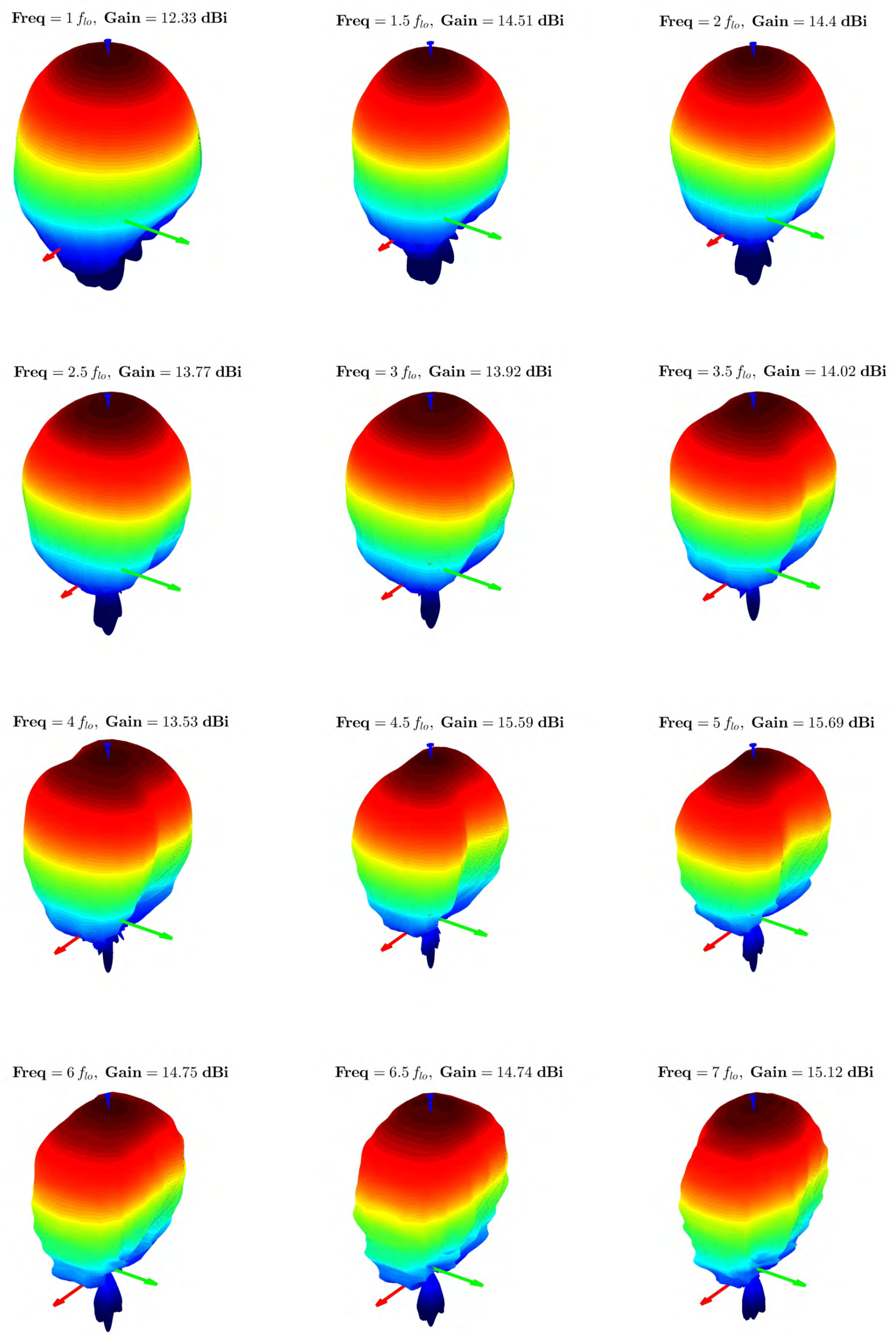

Figure 4.14: Three-dimensional radiation patterns of the high-gain QRFH

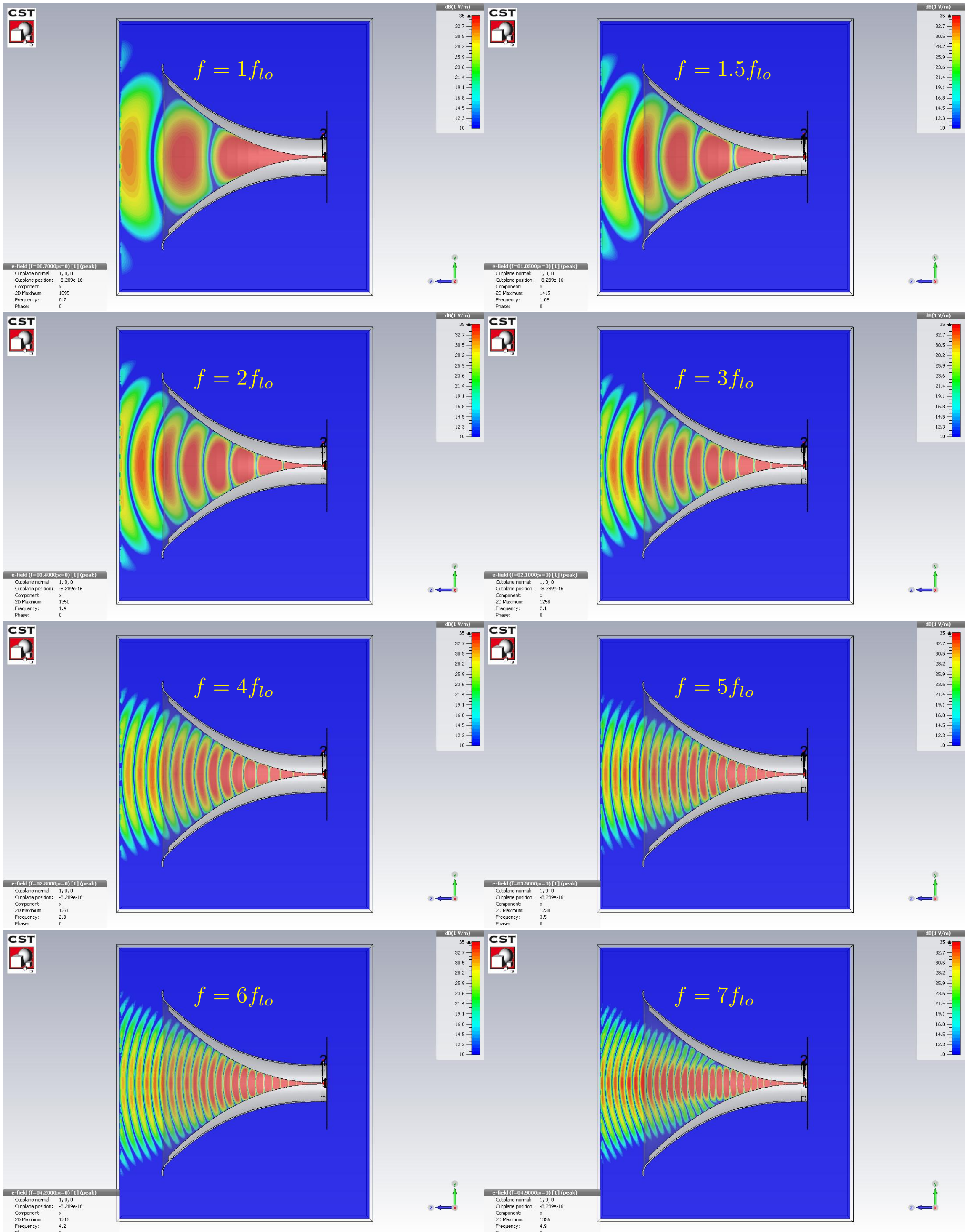

Figure 4.15: Intensity plots of E_x on the $x = 0$ plane in the high-gain quad-ridge horn which is excited in the x-polarization

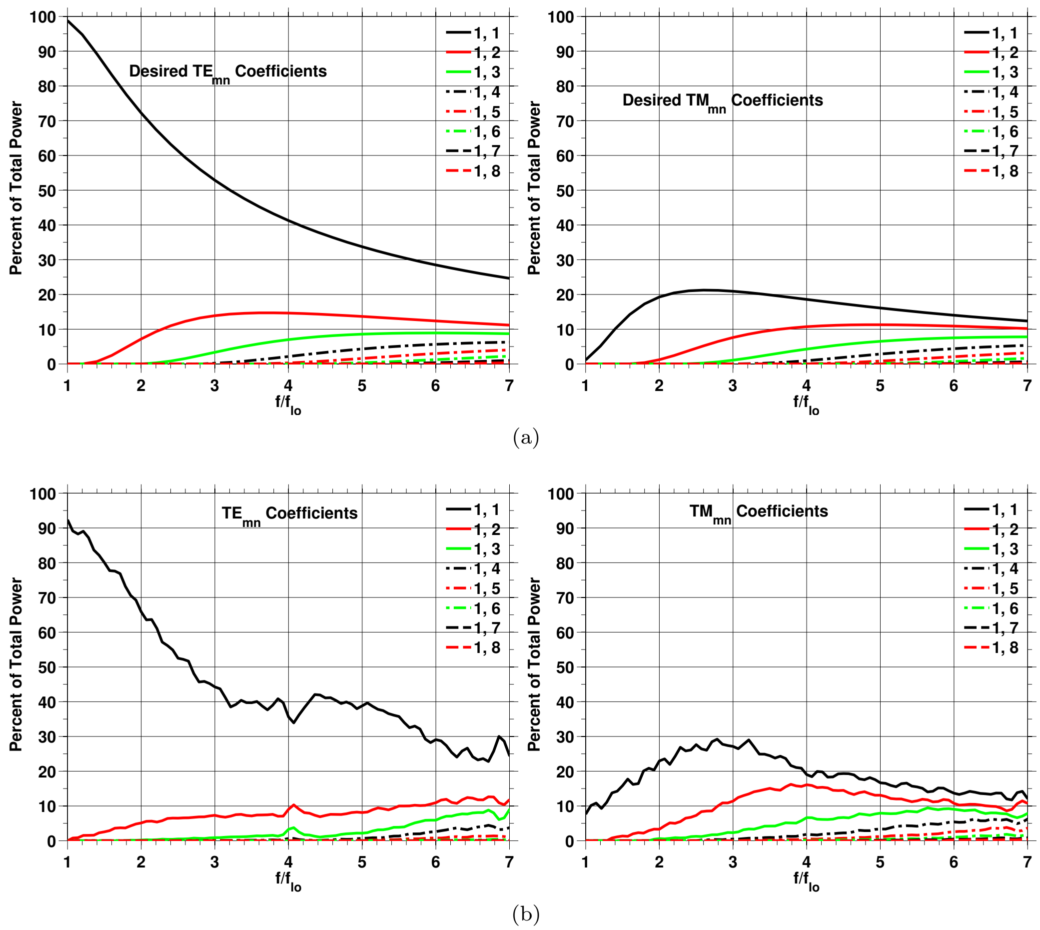

Figure 4.16: Normalized mode coefficients (a) required to achieve the desired radiation pattern, (b) at the aperture of the high-gain QRFH calculated using the simulated patterns. While all the modes present in the horn are not plotted, the modes plotted account for well more than 99% of the total power.

definition [33]) far-field patterns in $\phi = 0°$, $45°$, $90°$ planes and the three-dimensional, total radiation patterns are provided in Figure 4.14. The 10 dB beamwidths in E- and D-planes—and the azimuthal planes in between—are on average 65 degrees and the beamwidth stability is good. On the other hand, the H-plane beamwidth decreases from 80 to 40 degrees with increasing frequency resulting in a more elliptical beam at the upper end of the band. The cross-polarization in the D-plane peaks to -9 dB over narrow frequency ranges, and is below -10 dB over much of the band.

The intensity plots of E_x shown in Figure 4.15 once again shows tighter coupling to the ridges at the low end of the frequency band. There is discernible disruption of the fields at $7f_{lo}$ near the middle of the horn that could be due to undesired mode coupling. This could also be correlated with the decreasing return loss predicted by the simulations.

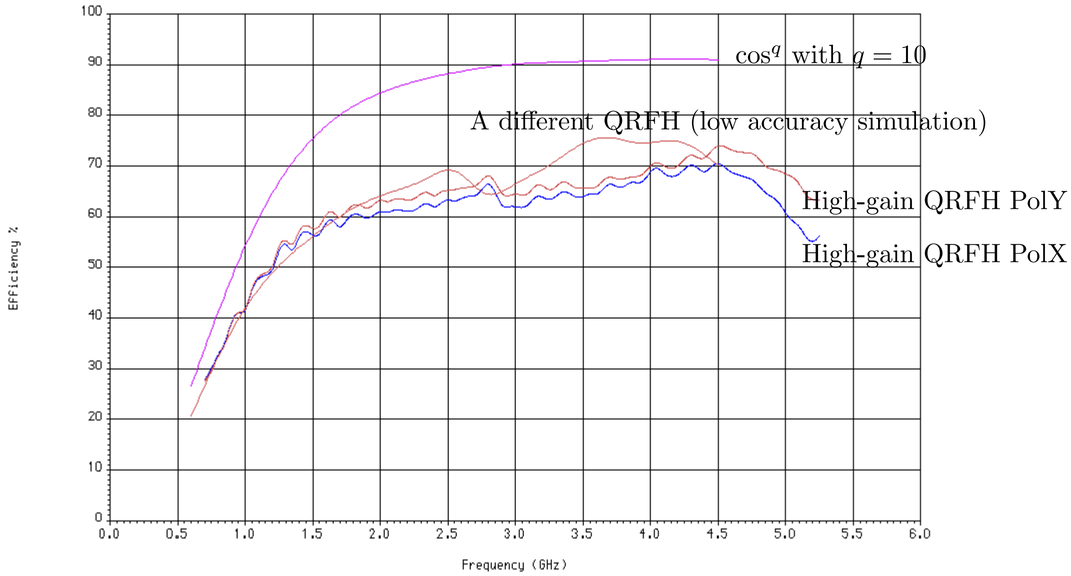

Figure 4.17: Predicted aperture efficiency of GAVRT with the high-gain QRFH as the feed antenna. The efficiency is calculated using physical optics and losses due to RMS surface error, blockage, struts, etc., are ignored.

4.3.3 Aperture mode content

Figure 4.16(a) and (b) plot, respectively, the calculated aperture mode coefficients of the high-gain QRFH and the mode coefficients required to achieve the desired radiation pattern, circularly symmetric far-fields with 10 dB beamwidth of 65 degrees. This design performs better compared to the very high gain QRFH with regards to achieving a mode distribution as close as possible to the desired one, the TM coefficient amplitudes showing especially significant improvement. Once again, the lack of even-order azimuthal modes is noted. Moreover, the mode coefficients exhibit smoother variation with frequency. The dip in TE_{11} amplitude—and the increase in TE_{12} and TE_{13} amplitudes—near $4f_{lo}$ corresponds to a similar drop in aperture efficiency presented in the next subsection.

4.3.4 Predicted system performance

Aperture efficiency of the Goldstone Apple Valley Radio Telescope with the high-gain quad-ridge as the feed antenna has been calculated from 0.7 to 5.2 GHz using physical optics. The calculations use simulated patterns and neglect losses due to RMS surface errors, blockage, struts, etc.

Figure 4.17 presents the aperture efficiency of both polarizations in addition to the maximum attainable aperture efficiency which is realized by $\cos^q$ feed pattern with $q = 10$. Also plotted in the same figure is aperture efficiency of the telescope with an earlier QRFH design that works at lower frequencies than the high-gain horn presented herein. The modeled efficiency is between 60 to 70%

from about 1.5 to 5 GHz on both polarizations. The efficiency roll-off at the low end of the band is due to the tertiary mirror being too small in terms of wavelength and not due to the horn. While the antenna noise temperature has not been calculated in this case, it is reasonable to expect very low spillover pick-up due to two reasons: 1) the quad-ridge horn under-illuminates the tertiary for most of the band; 2) spillover energy does not see the earth, but instead gets reflected from the primary mirror and radiates into space. Therefore, for most elevation angles the antenna noise temperature is expected to be less than 10 K.

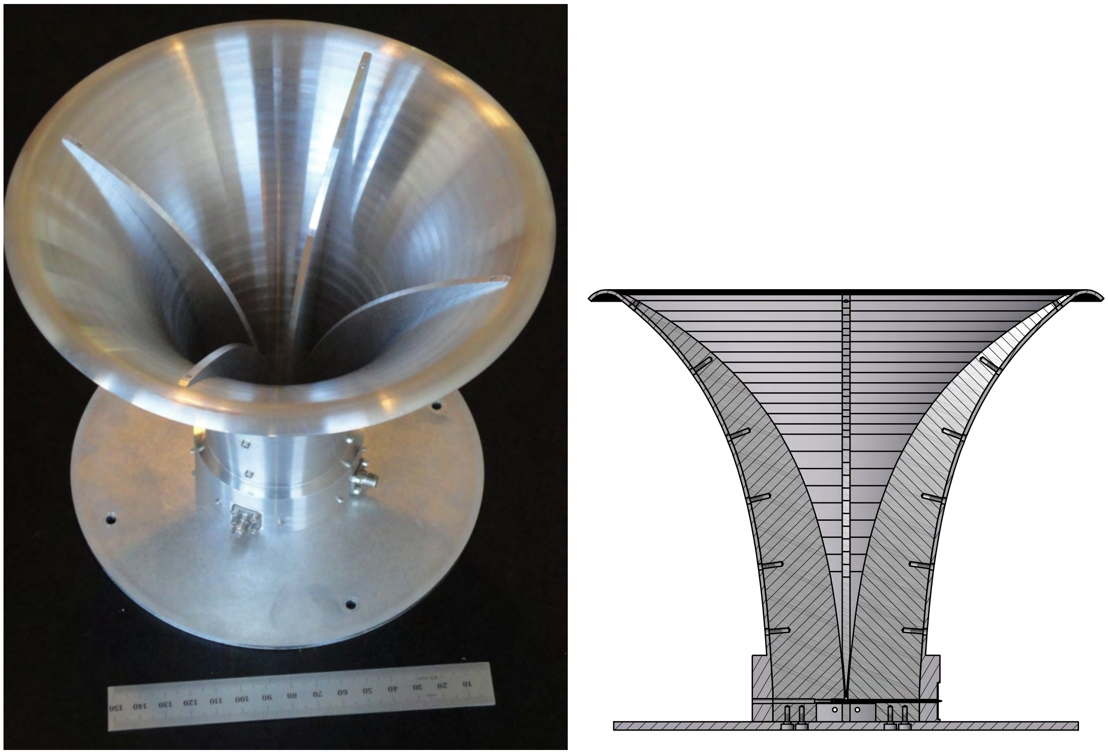

Figure 4.18: A photo and three-dimensional CAD drawing of the medium-gain quad-ridge horn. Feed diameter is 18 cm ($1.2\lambda_{lo}$) and length is 16.4 cm ($1.1\lambda_{lo}$) with $f_{lo} = 2$ GHz.

4.4 Medium-Gain QRFH

4.4.1 Application

The shaped dual-reflector radio telescope, for which the medium-gain QRFH is designed, was built with optics designed at the Jet Propulsion Laboratory [56] and mechanical design and construction by Patriot/Cobham. The primary reflector has a diameter of 12 meters and the full subtended angle to the secondary reflector is 100 degrees. It is located at the Goddard Geophysical and Astronomical Observatory (GGAO), where it serves as a radio telescope for a geodetic VLBI application requiring 50% aperture efficiency and 50 Kelvin system noise temperature.

4.4.2 Stand-alone measurements

The quad-ridge horn is designed with nominal 10 dB beamwidth of 90 degrees and the target frequency band is 6:1. Both the ridge and sidewall tapers use the exponential profile with an aperture diameter of $1.18\lambda_{lo}$ and the horn length of $1.09\lambda_{lo}$. The measured reflection coefficients and isolation are plotted in Figure 4.19. The measured isolation is better than 30 dB up to $10f_{lo}$, which is higher than the simulated isolation (not plotted for clarity) of 40 dB up to $7.5f_{lo}$. The return loss is better than 10 dB up to almost $10f_{lo}$ for both ports and significantly better than 15 dB over

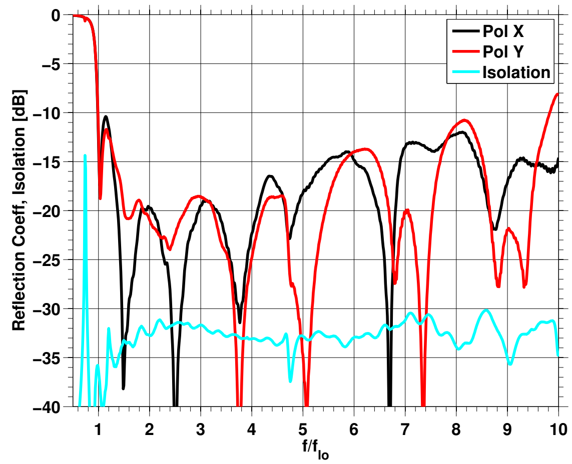

Figure 4.19: Measured scattering parameters of the medium-gain QRFH

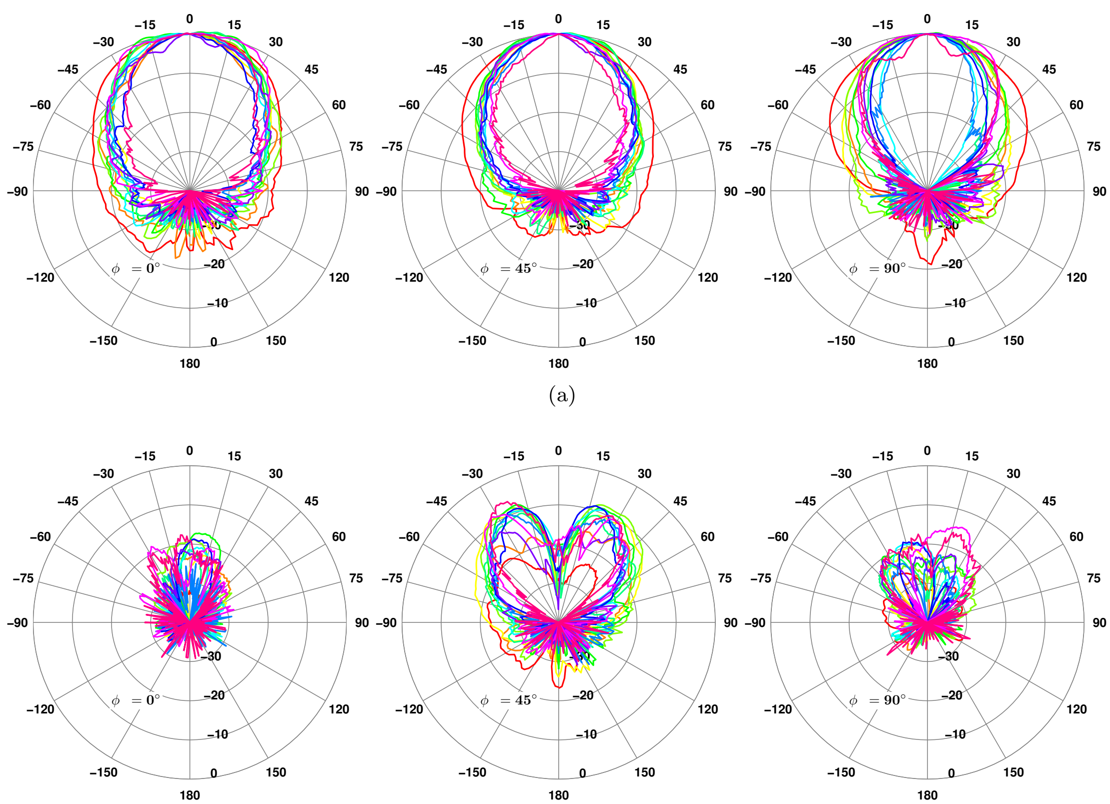

(a)

(b)

Figure 4.20: Measured (a) co-polarized, (b) cross-polarized (Ludwig 3rd definition) radiation patterns of the medium-gain QRFH in $\phi = 0°$, $45°$, $90°$ azimuthal planes over the frequency range $f/f_{lo} = [1,\ 6]$

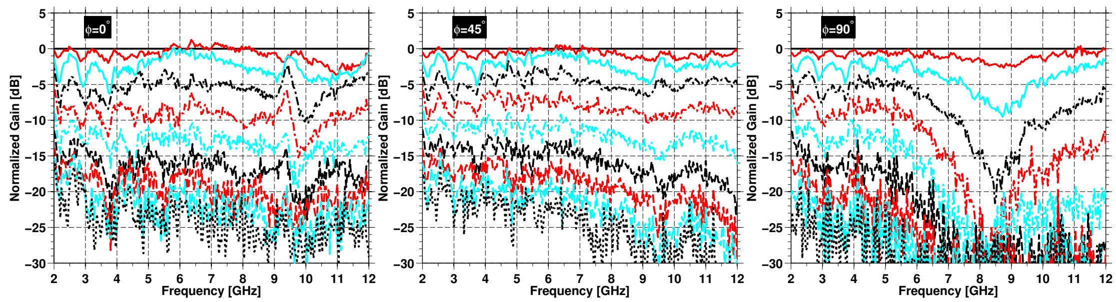

(a)

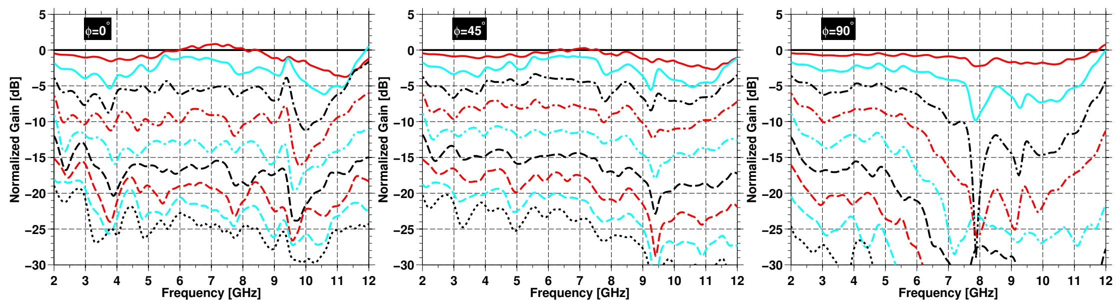

(b)

Figure 4.21: Comparison of (a) measured and (b) simulated co-polarized radiation patterns of the medium-gain QRFH in $\phi = 0°$, $45°$, $90°$ azimuthal planes over the frequency range $f/f_{lo} = [1, 6]$. The curves are at θ angles from 0 to 90 degrees in steps of 10 degrees and are normalized to $\theta = 0°$.

majority of the band.

The normalized radiation patterns of the QRFH are plotted in Figure 4.20 up to $6f_{lo}$ in the E-, D- and H-planes and the simulated three-dimensional patterns are presented in Figure 4.22. Good beamwidth stability is noted in both E- and D-planes. Like the other quad-ridge horns, H-plane beamwidth shows more variability because of the different boundary condition on the magnetic fields in the horn. The peak cross-polarization, similar to the horns described previously, is around -10 dB.

Figure 4.21 compares measured and simulated patterns in the three azimuthal planes which demonstrates that the CST MWS does an excellent job estimating the far-zone radiation patterns of the QRFH. Most of the fine features in the measurements are captured by the simulations. This figure also indicates that high-frequency ripple in measured patterns is an artifact of the far-field range and not due to the horn.

Simulated intensity plots of E_x in Figure 4.23 highlight the fact that both the aperture diameter and the horn length are small in terms of wavelength at the low end of the band. Energy leaking in the back direction around $2f_{lo}$ results in increased backlobes, approximately 18 dB below boresight according to the simulations; however, this is not observed in the measured patterns which could be due to the mounting plate used during tests. There is also some minor field disruption at $6f_{lo}$, which may be correlated with the beam widening observed in the three-dimensional patterns.

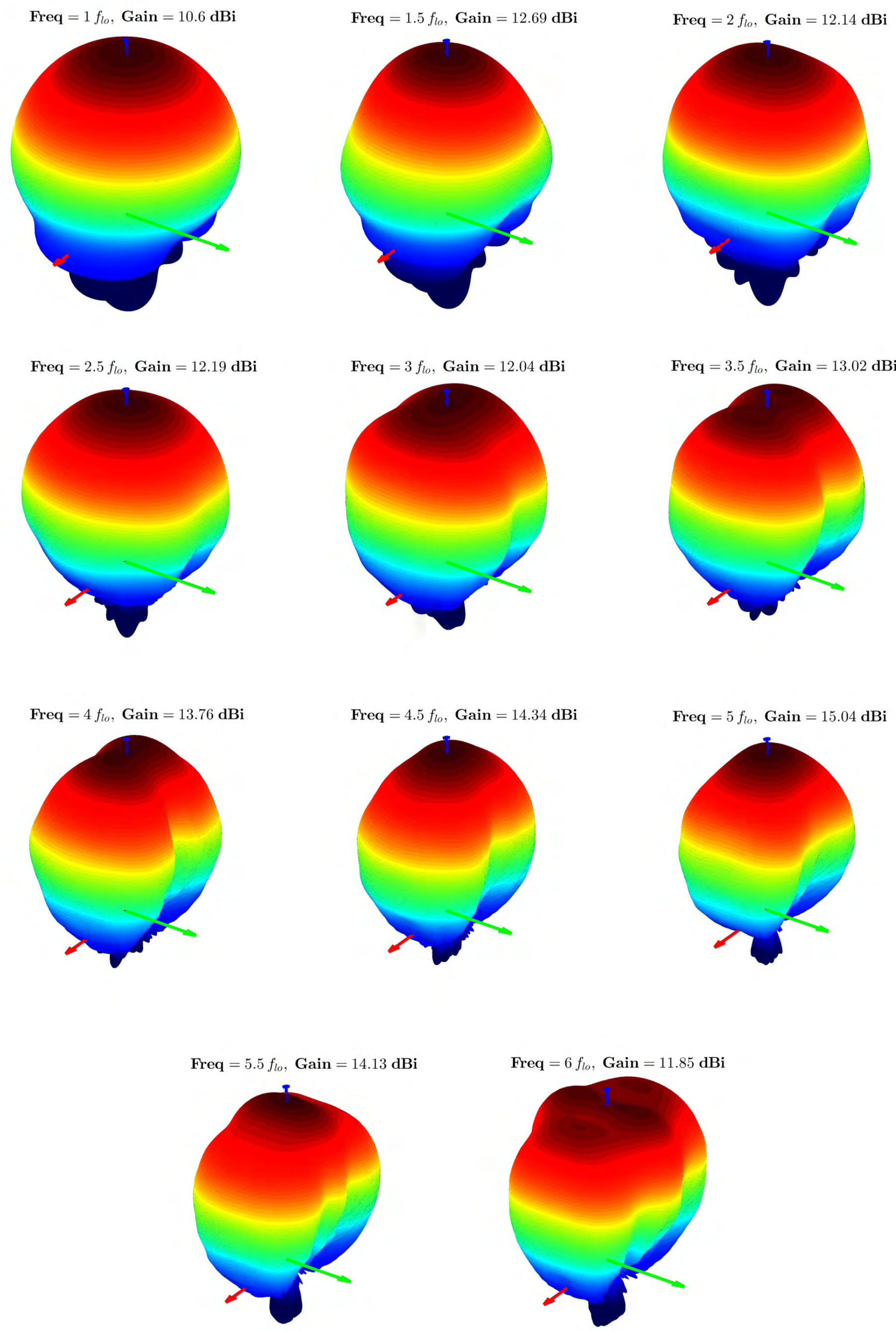

Figure 4.22: Three-dimensional simulated far-field patterns of the medium-gain QRFH.

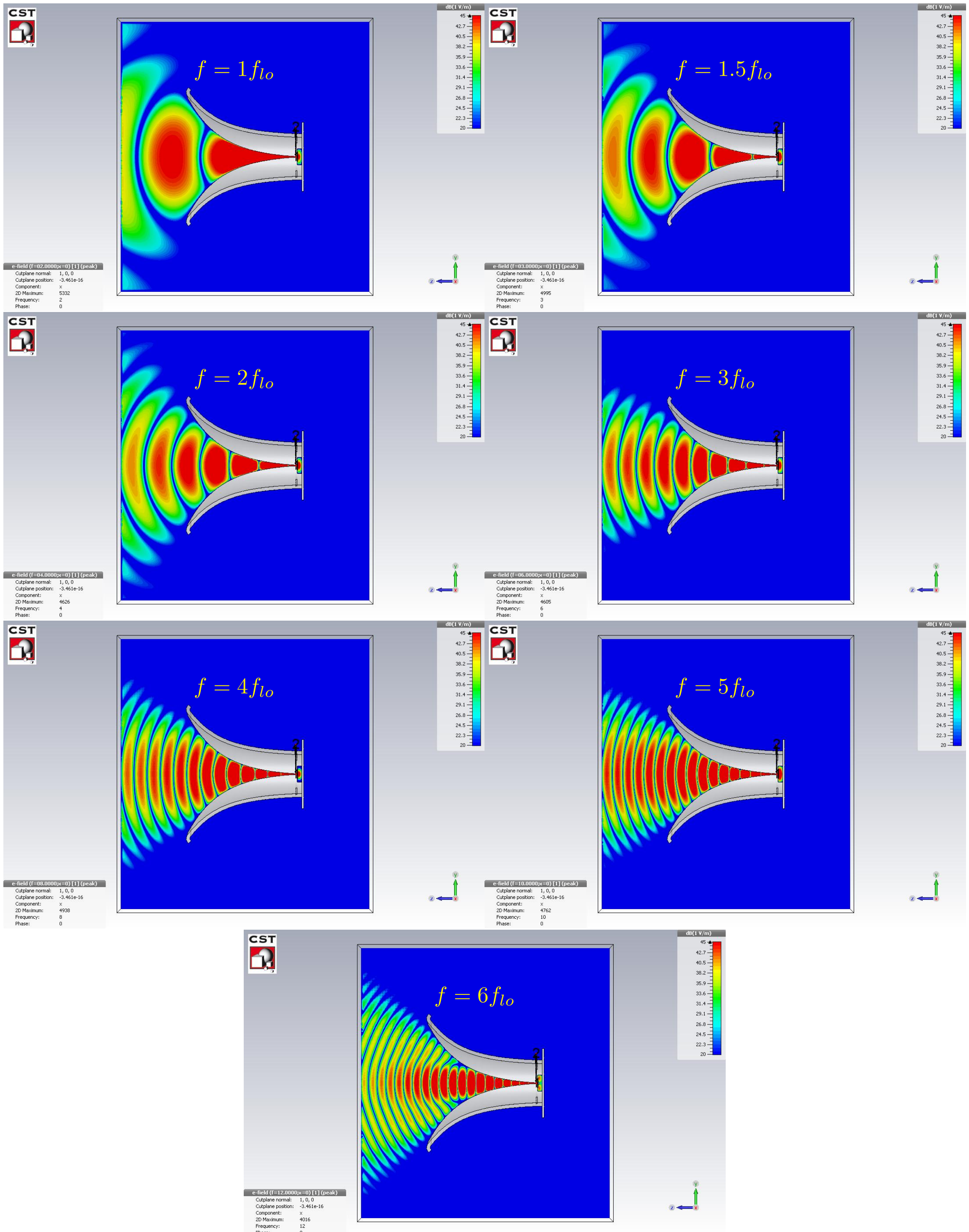

Figure 4.23: Intensity plots of E_x on the $x = 0$ plane in the medium-gain quad-ridge horn which is excited in the x-polarization.

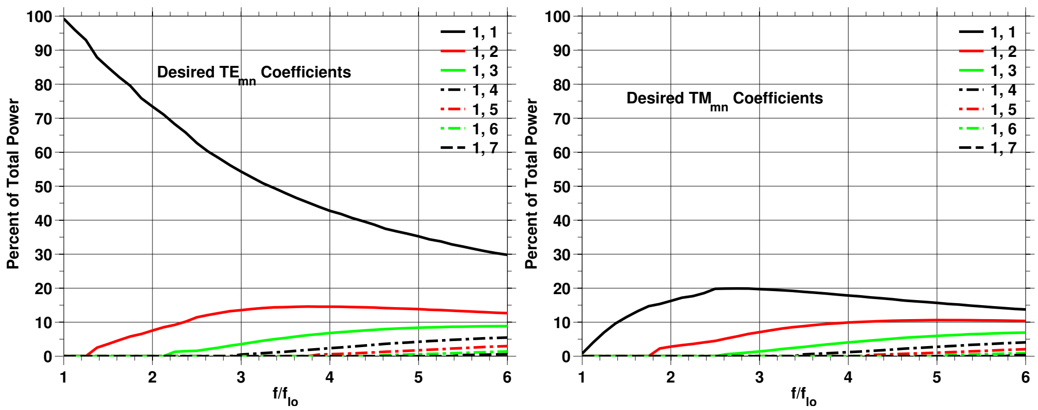

(a)

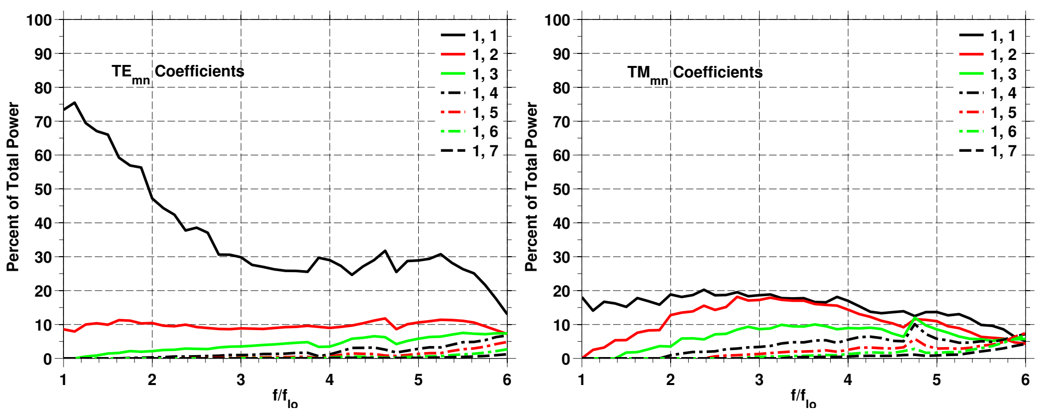

(b)

Figure 4.24: Normalized mode coefficients (a) required to achieve the desired radiation pattern, (b) at the aperture of the medium-gain QRFH calculated using the simulated patterns. The first 7 TE and 7 TM modes are plotted, which carry the vast majority of the power in the aperture. The simulated patterns are used, instead of measurements, because of higher azimuthal resolution.

4.4.3 Aperture mode content

Figure 4.24 presents the aperture mode analysis results in part (a) and the necessary mode amplitudes in part (b). The achieved TE_{11} amplitude is considerably lower than the desired amplitude at the low end of the band with the TE_{12} and TM_{11} modes mostly carrying the power difference. This disparity is likely due in part to the aperture being too small in terms of wavelength at these frequencies and the error due to assumptions in the mode calculation (see Appendix 3.5) could be significant. Another interesting observation not seen on the previous two horn designs is that the TE_{12} mode carries roughly the same fraction of the total power regardless of frequency. It is below cutoff at the feed point of the horn all the way up to approximately 8 GHz which suggests that it is generated by curvature of ridges and sidewall and is not excited significantly at the feed point.

4.4.4 System measurements

The block diagram of the 2-14 GHz broadband receiver installed on the 12m telescope is shown in Figure 4.25(b). The QRFH is followed by two broadband stripline couplers and two cryogenic low-noise amplifiers (also developed at Caltech) which are all located inside the cryogenic dewar (see right half of Figure 4.25(a)) and are cooled to 20 Kelvin physical temperature during telescope operation. The couplers, despite being cooled, increase overall system noise temperature by a small amount and are necessary to calibrate the system gain and phase.

The microwave outputs of the LNAs are then passed through two power dividers in order to split the low-frequency and high-frequency bands due to strong S-band radio frequency interference and thereby increase dynamic range beyond 4 GHz. The system results presented here are from the high-frequency band which, as shown in the block diagram, employs 4 GHz high-pass filters. Due to the total RF bandwidth available from the front-end, the sheer volume of back-end electronics makes it prohibitive to collocate them with the RF front-end near the apex of the primary reflector. Instead, a microwave-over-fiber link, which provides fairly uniform insertion loss up through 14 GHz, is employed to bring the microwave signals down to the electronics room housing the down-converter and subsequent digital electronics.

To assess the sensitivity of the GGAO 12m radio telescope, a broadband system equivalent flux density, $SEFD\left(f\right)$, was measured. It is the source flux which will produce a receiver power output equal to that produced by the system noise and is measured by moving the telescope on and off a source of known flux as described as follows:

$$SEFD\left(f\right) = \frac{P_{off}\left(f\right)}{P_{on}\left(f\right) - P_{off}\left(f\right)} \frac{S_{src}\left(f\right)}{\Delta\left(f\right)} \tag{4.1}$$

where f is frequency. In this technique, the telescope observes a radio source of known broadband flux $S_{src}\left(f\right)$ in units of Jansky and the on-source power spectrum, $P_{on}\left(f\right)$, is measured by the broadband radio receiver. Then, the off-source power spectrum, $P_{off}\left(f\right)$, is measured with the antenna pointed off source azimuthally (to maintain constant atmospheric noise) by 3 beamwidths at the lowest observation frequency. The source size correction factor, $\Delta\left(f\right)$, compensates for the fact that the antenna beam is not large enough to collect all the flux from the target radio source.

The SEFD estimates of the GGAO 12m telescope were obtained using Cassiopeia A (Cas A) as the radio source calibrator. The frequency dependent source flux of Cas A is given by [57, 58]:

$$\log_{10}\left[S_{src}\left(f\right)\right] = 5.745 - 0.770\log_{10} f \tag{4.2}$$

with frequency f in MHz. The source flux density also needs to be corrected for the secular decrease

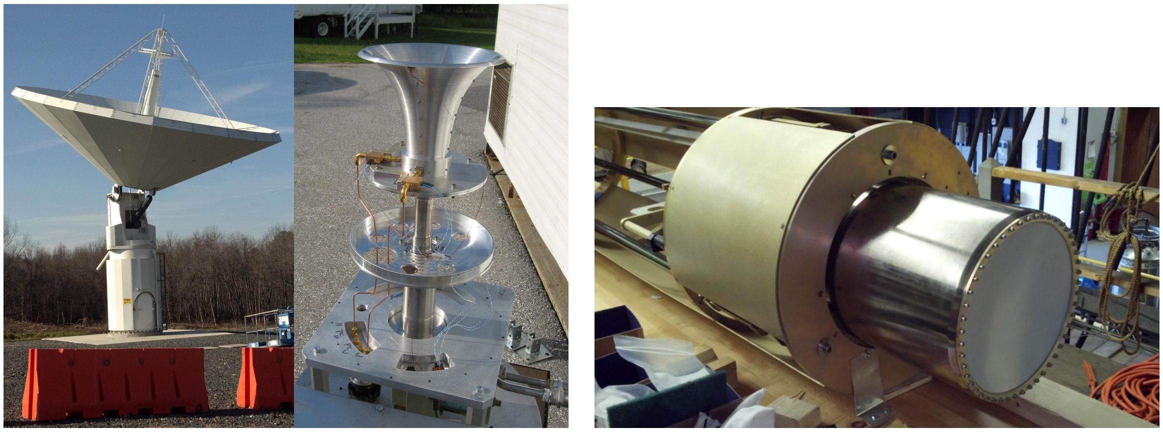

(a)

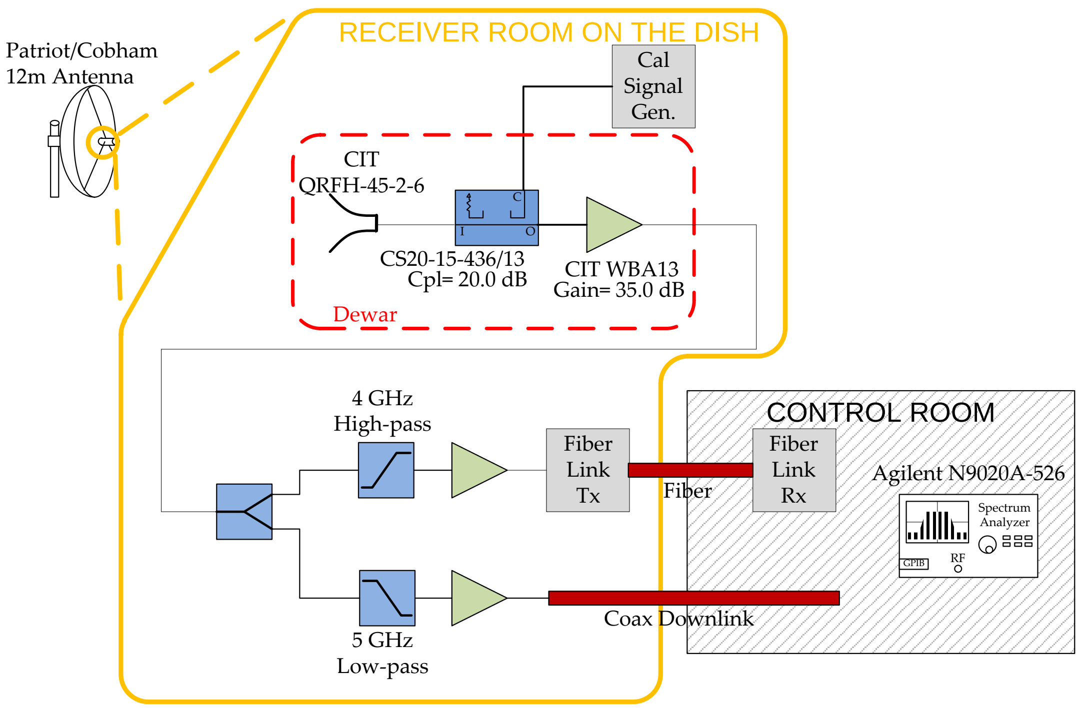

(b)

Figure 4.25: (a) 12 meter Patriot antenna at GGAO (left) and integration of the circular QRFH into the dewar (calibration couplers not shown; right), (b) block diagram of the 12 meter radio telescope front-end showing RF electronics for one linear polarization only.

in flux density of Cas A whose percentage value per year is given by [58]

$$d(f) = 0.97 - 0.3\log_{10} f - 3 \tag{4.3}$$

with f in MHz again. The radio source structure of Cas A is modeled with a disk source distribution, the form of the source size correction factor for such a model is given by [57, 59]:

$$\Delta(f) = \frac{x^2}{1 - e^{-x^2}} \text{ with } x = \sqrt{4\ln 2} \times \frac{R}{\theta_{HPBW}} \tag{4.4}$$

where R is the angular radius of the disk and is 2.15 arcminutes [57], and θ_{HPBW} is the half-power beamwidth of the telescope.

An Agilent N9020A-526 signal analyzer was used as the broadband radio receiver for the sensitivity evaluation. In these experiments, the signal analyzer was configured to collect power spectrum measurements from 2-14 GHz with a 3 MHz resolution bandwidth. Power spectrum measurements were collected with the telescope both on and off the radio source and stored on hard disk for subsequent data processing. In order to reduce trace noise in the measurements and in turn enhance the precision in the SEFD estimate, a sliding window filter of length of approximately 100 MHz was applied to both on- and off-source data sets in post processing.

The broadband source equivalent flux density measurements with Cas A were conducted and equations (4.1)-(4.4) were used to compute the SEFD to estimate the telescope sensitivity. Converting the SEFD estimate to more familiar aperture efficiency requires knowledge of system noise temperature T_{sys} and is accomplished via:

$$A_{eff} = \frac{2kT_{sys}}{SEFD(f) \cdot \pi r^2} \times 10^{26} \tag{4.5}$$

where k is Boltzmann's constant and r is radius of primary reflector. The system noise temperature is defined as

$$T_{sys} \equiv T_{Rx} + \underbrace{T_{sky} + T_{spillover}}_{T_{antenna}} \tag{4.6}$$

where the terms on the right-hand side are, in order from left to right, receiver, sky, and spillover noise temperatures. The T_{sys} is calculated using the Y-factor method with hot/cold loads and is given by

$$T_{sys} = \frac{T_{hot} - YT_{cold}}{Y - 1}. \tag{4.7}$$

The hot load used for these tests is an ambient temperature RF absorber with measured physical temperature T_{hot}, of the order of 295 K, and the Y-factor is given by the ratio of receiver output power with hot load to that with cold load, i.e., P_{hot}/P_{cold}. The cold load measurements is performed

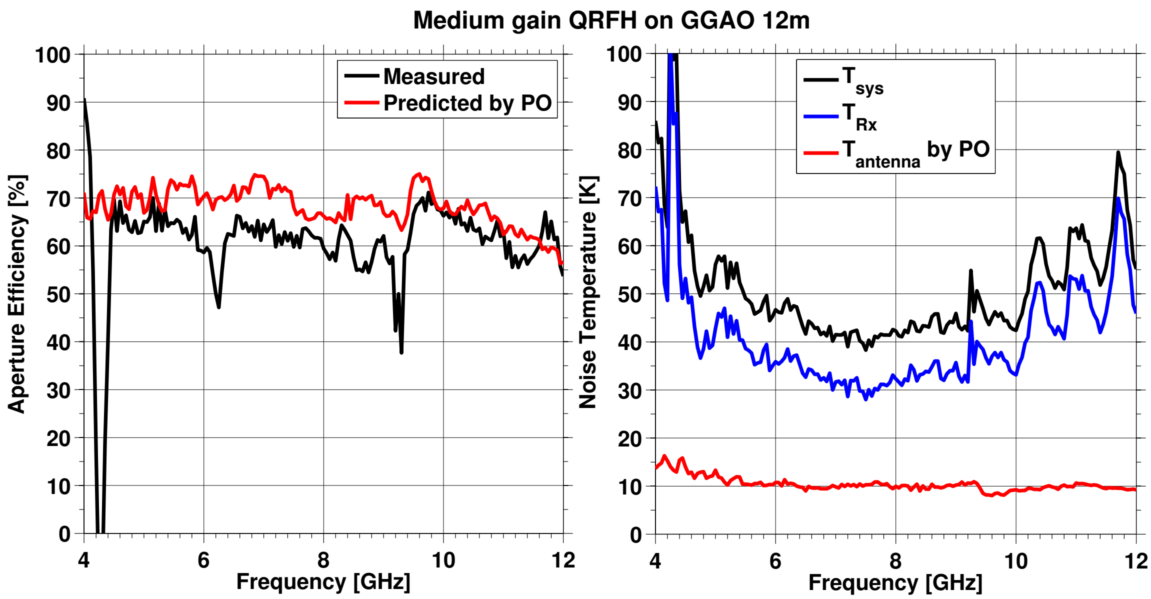

Figure 4.26: The measured system noise temperature and aperture efficiency of the circular QRFH installed on the GGAO 12 m telescope. The predicted aperture efficiency and antenna noise temperature—both based upon QRFH far-field pattern integration—are also plotted. The sky noise temperature is calculated per the method outlined in [60], and is 5.5K at 4 GHz and 6.5K at 10 GHz.

by pointing the telescope off the radio source instead of using an actual liquid nitrogen termination. As such, $T_{cold} = T_{sys}$ which gives

$$T_{sys} = \frac{295 - T_{sky} - T_{spillover}}{Y - 1} \tag{4.8}$$

Without the knowledge of T_{sky} and $T_{spillover}$, this equation cannot be solved to obtain T_{sys}. Consequently, the sky and spillover noise temperatures are estimated by using predicted values from physical optics calculations as explained below. The system noise temperature measurements are carried out in the same configuration as SEFD observations, namely with feed, couplers and LNAs in the dewar on the telescope followed by the fiber link and the associated back-end electronics.

Using (4.5), the measured broadband aperture efficiency of the GGAO 12m antenna with the QRFH feed is plotted in Figure 4.26. Also plotted in the same figure are predicted aperture efficiency and spillover and sky noise temperatures curves based upon the QRFH pattern measurements. A custom physical optics program, which takes into account shaping of both reflectors, was used to compute all three quantities with the spillover and sky noise temperatures computed at 48 degree elevation angle. On the other hand, the Cas A SEFD measurements were performed at an elevation angle of 60 degrees; however, because spillover and sky temperatures do not usually change rapidly with elevation angle, the predicted spillover and sky temperatures at 48 degree elevation are used to estimate the receiver noise contribution.

The measured aperture efficiency is better than 60% up to 8 GHz and stays above 54% up to 12 GHz. Aperture efficiency averaged over the entire band is 60%. The dips in efficiency near 4, 6 and 9 GHz are not due to the horn, but rather are likely artifacts of interference. This is the first demonstration of a quad-ridge horn achieving such good performance on a radio telescope. The measured efficiency is in very good agreement with the efficiency calculated by physical optics using the measured antenna patterns. The fairly small difference between the predictions from physical optics and the measurements is most likely due to blockage by the subreflector and its struts.

The measured system noise temperature is better than 50 K from 5 to 10 GHz and is mostly dominated by the receiver temperature. The Caltech LNAs achieve between 5-20 K noise in this band where the noise degradation is due to protection diodes. There is an estimated 1 dB loss preceding the LNA in addition to 3 K additional noise through the coupled arm of the directional coupler due to finite directivity. Taking all of this into account, there remains about $\geq$ 10 K discrepancy between estimated T_{Rx} and that suggested by measurements. At this point, the source of this discrepancy is unclear, but is thought to be one or more of the following:

1. increased $T_{antenna}$ due to scattering off of struts and other supporting structures of the reflector. It is very unlikely the additional noise is due to feed loss because the theoretical loss of the feed, mostly in the internal coaxial lines, is of the order of 0.1dB, and this would contribute only 0.5K with the feed at 20K.

2. Cryogenic losses, especially preceding the LNAs, unaccounted for in the existing analysis.

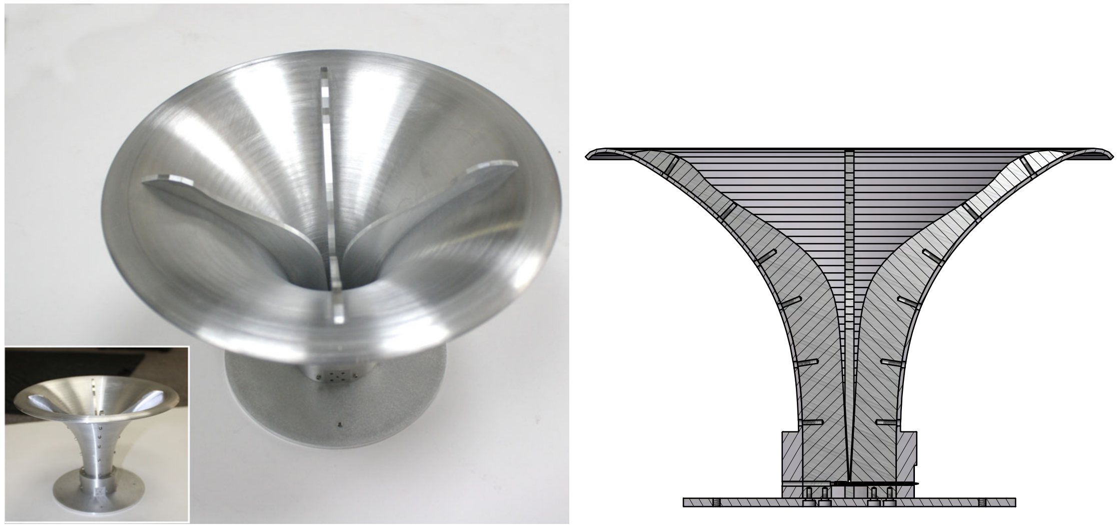

Figure 4.27: Photo and three-dimensional CAD drawing of the low-gain QRFH. Feed diameter is 20 cm ($1.5\lambda_{lo}$) and length is 13.4 cm ($1.03\lambda_{lo}$) with $f_{lo} = 2.3$ GHz.

4.5 Low-Gain QRFH

4.5.1 Application

This QRFH is intended for telescopes with $f/D \approx 0.4$. The first of this design has been built and tested and is in the process of being integrated into a VLBI2010 [2] front-end in Japan. Two more identical horns are being built, one for MIT Haystack Observatory and the other for Shanghai Astronomical Observatory.

The telescope in Japan, on which this QRFH will be installed, is a copy of the so-called Twin-Telescope Wettzell, designed and fabricated in Germany [61]. It has a ring-focus secondary mirror with a primary mirror diameter of 13.2 meters and an effective f/D of approximately 0.4.

4.5.2 Stand-alone measurements

The quad-ridge horn ridge taper uses the sinusoidal profile while the sidewall taper follows the x^p functional form. The nominal 10 dB beamwidth is 120 degrees and the desired bandwidth is 6:1. The horn length is about $1\lambda_{lo}$ and the aperture diameter is $1.12\lambda_{lo}$ with a flare angle of 55 degrees.

The measured reflection coefficients of both polarizations are plotted in Figure 4.28 along with the isolation. Except between 1.2 and $1.6f_{lo}$, the return loss is 15 dB or better across most of the band for both polarizations, and the isolation is better than 25 dB. The increase in return loss between 1.2 and $1.6f_{lo}$ was predicted by simulations and was a conscious design choice.

Figure 4.29 presents the measured patterns in polar format for the E-, D-, and H-planes. The three-dimensional patterns are plotted in Figure 4.30. One of the first observations is that the beamwidth in D-plane is not as constant as the higher gain QRFHs presented herein and it is

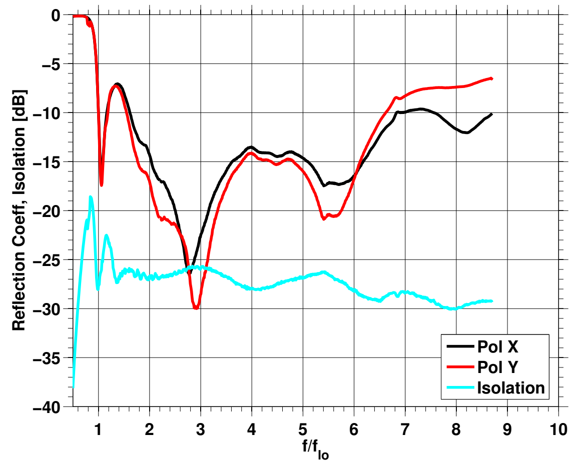

Figure 4.28: Measured scattering parameters of the low-gain QRFH

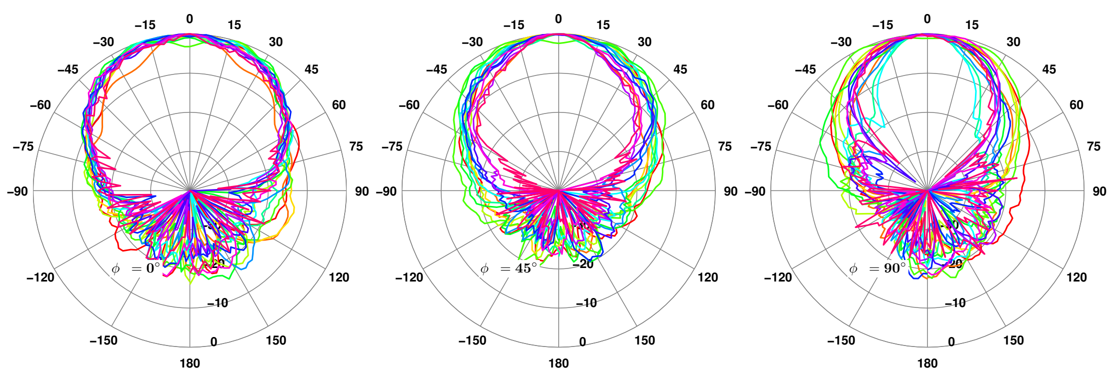

(a)

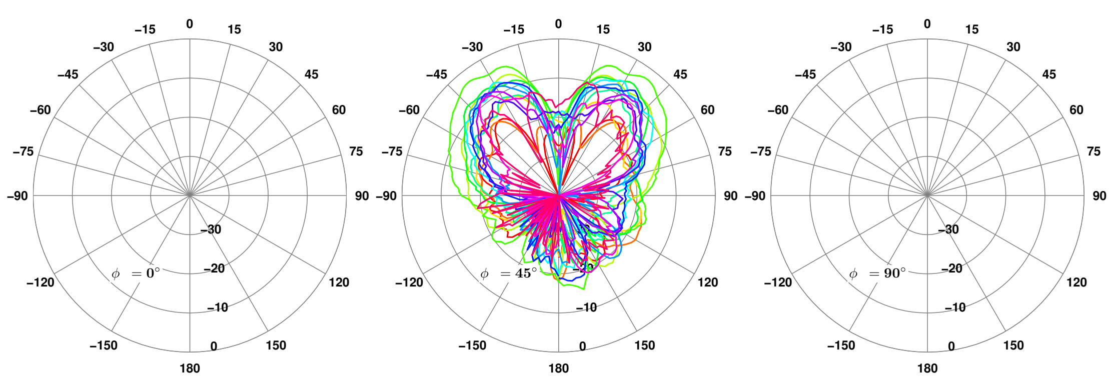

(b)

Figure 4.29: Measured (a) co-polarized, (b) cross-polarized (Ludwig 3rd definition) radiation patterns of the low-gain QRFH in $\phi = 0°, 45°, 90°$ azimuthal planes over the frequency range $f/f_{lo} = [1,\, 6]$

on average narrower than the beamwidth in the E-plane which is 120 degrees. Like the other quad-ridge horns, the H-plane shows significantly more variation. The asymmetry in the radiation patterns between θ around -90 degrees and 90 degrees is due to the pattern measurement setup. The roof wall is at $\theta = 90$ degrees causing this beam widening artifact in the measurements. The cross-polarization level of this horn peaks to -5 dB over very narrow frequency range with a nominal level of -8 to -9 dB which is higher than previous designs.

The intensity plots of E_x in Figure 4.31 show similar features as the other horns. Comparing the intensity plots of the higher gain horns to those of the lower gain ones, one observes significant difference between curvatures of the wave fronts in the two cases. The lower gain horns exhibit more curvature and the fields are coupled fairly strongly to the ridges even near the aperture. These are most easily noticed at mid to upper end of the frequency band. On the other hand, the higher gain horns usually have more planar wave fronts and the fields are loosely coupled to the ridges near the aperture.

4.5.3 Predicted system performance

Aperture efficiency of the 13.2 meter ring-focus telescope is computed using physical optics ignoring losses due to blockage, struts, rms surface errors, etc. The simulated patterns are used in the calculations, which is justified by the close agreement between modeling and measurements of this horn. Antenna noise temperature is also computed, using the method described in [60, 62], for the telescope pointing near zenith. Both efficiency and noise temperature are calculated from 2 to 15 GHz as the frequency band of interest in VLBI2010 applications is 2.3 to 14 GHz.

Figure 4.32 presents the computed aperture efficiency and the antenna noise temperature in parts (a) and (b), respectively. Also plotted in this figure are the efficiency and antenna noise temperature of the telescope with the medium-gain QRFH presented herein as the feed antenna. The efficiency with the low-gain QRFH is better than 50% all the way up to 15 GHz and the average efficiency in the frequency range of interest is $> 55\%$. The antenna noise temperature is also very good, less than 10 K from 2.5 to 15 GHz.

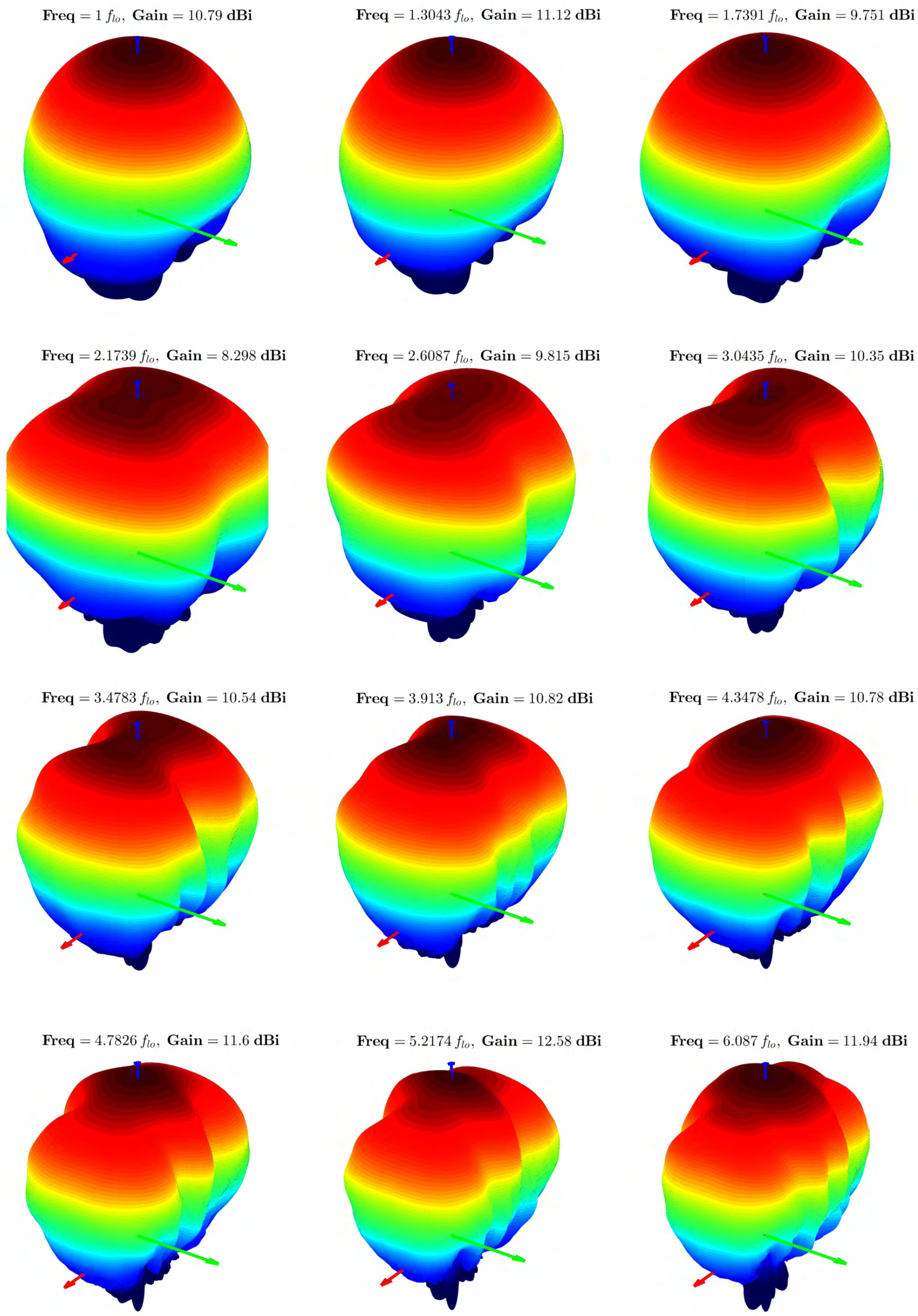

Figure 4.30: Three-dimensional simulated far-field patterns of the low-gain QRFH

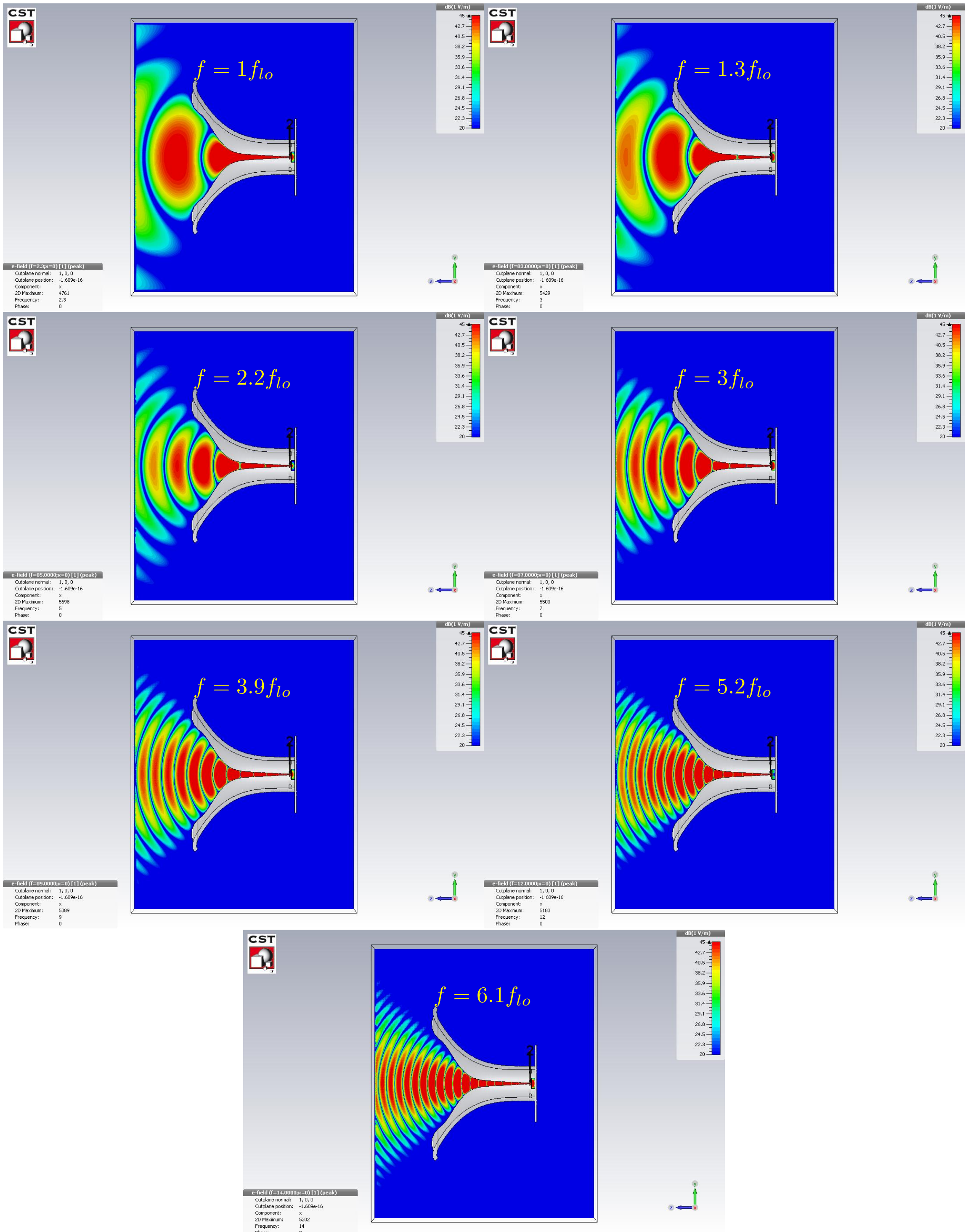

Figure 4.31: Intensity plots of E_x on the $x = 0$ plane in the low-gain quad-ridge horn which is excited in the x-polarization

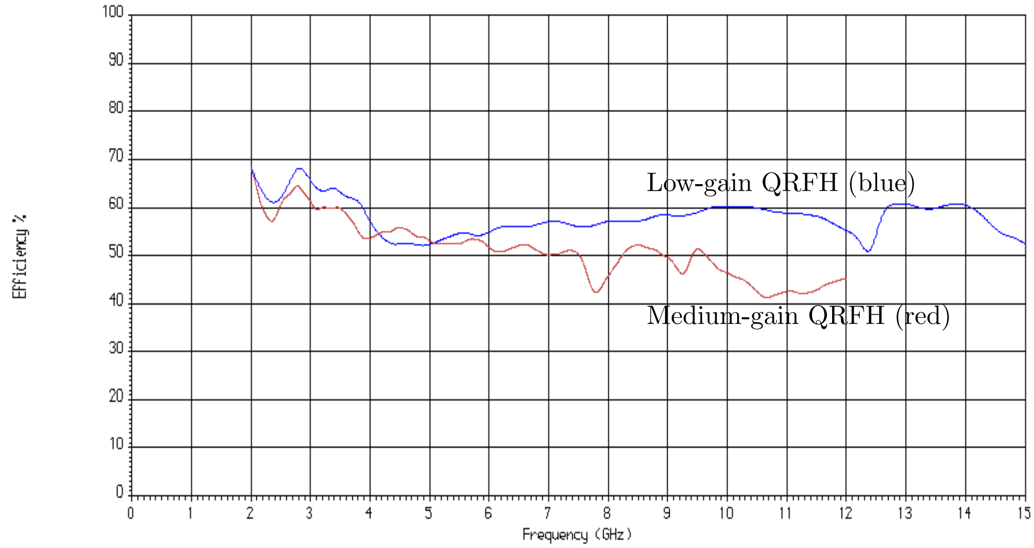

(a)

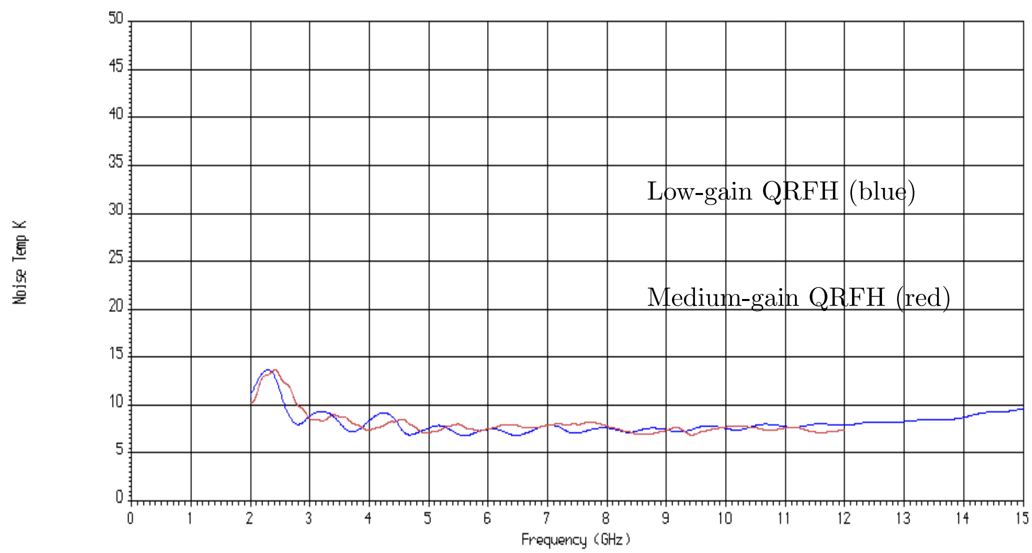

(b)

Figure 4.32: Predicted (a) aperture efficiency, (b) antenna noise temperature of the 13.2 meter ring-focus telescope with the low-gain (blue) and medium-gain (red) QRFH as the feed antenna. The efficiencies are calculated using physical optics and losses due to RMS surface error, blockage, struts, etc., are ignored. Telescope is assumed to point near zenith for noise temperature calculations.

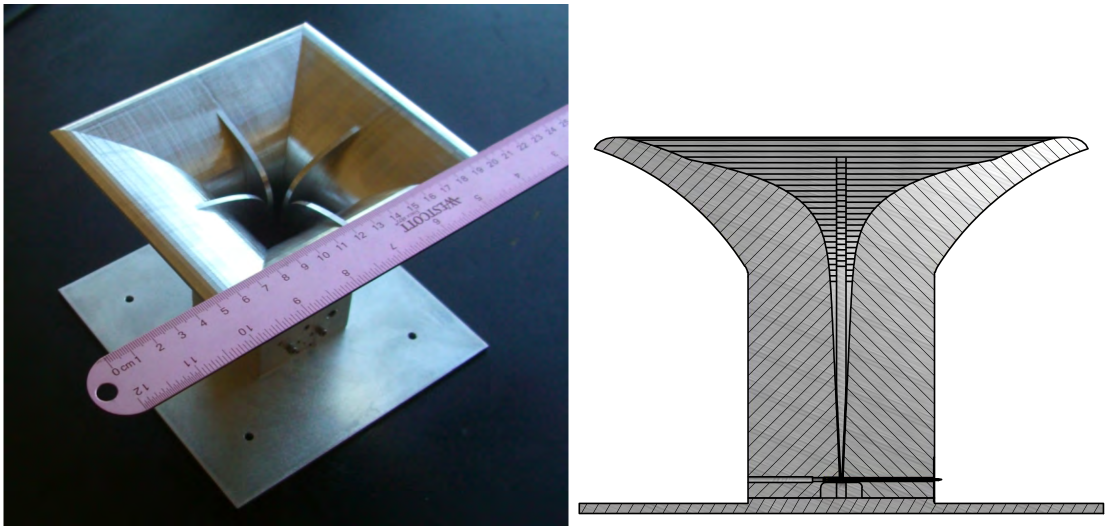

Figure 4.33: Photo and three-dimensional CAD drawing of the very low gain quad-ridge horn. Feed diameter is 14.3 cm ($1.1\lambda_{lo}$) and length is 11.9 cm ($0.91\lambda_{lo}$) with $f_{lo} = 2.3$ GHz.

4.6 Very-Low Gain QRFH

4.6.1 Application

The quad-ridge horn with the widest beamwidth is designed for the Westford Radio Telescope at MIT Haystack Observatory. It is a dual reflector system in Cassegrain configuration with a symmetric paraboloid primary mirror (diameter of 18.3 meters) and $f/D = 0.3$ [63]. The horn is currently integrated into a VLBI2010 receiver at MIT Haystack Observatory.

4.6.2 Stand-alone measurements

The unique aspect of this horn is that it is square instead of circular, see Figure 4.33 for a photo. Square horns are more favorable for low-frequency designs because they are only curved in one plane and thus, could be made out of sheet metal much more easily than circular horns. However, their disadvantage is the increased size at the aperture along the diagonal. The design uses exponential sidewall taper and x^p profile for the ridge taper. The nominal beamwidth is 140 degrees. The aperture side length is $1.05\lambda_{lo}$ and the horn length is $0.87\lambda_{lo}$. The flare angle is approximately 74 degrees. This is the smallest horn in terms of wavelength designed as part of this research.

The measured return loss of both polarizations and the simulated isolation (due to lack of measurement) are provided in Figure 4.34. The match is poor below $2f_{lo}$. This is similar to (and worse than) the low-gain design of the previous section in that only the low-frequency input match deteriorates. The reason low-frequency match degrades with increasing beamwidth is the reduction in aperture size and horn length. In other words, the horn is becoming too small in terms of wavelength which implies reflections from the aperture which, in turn, degrade input match.

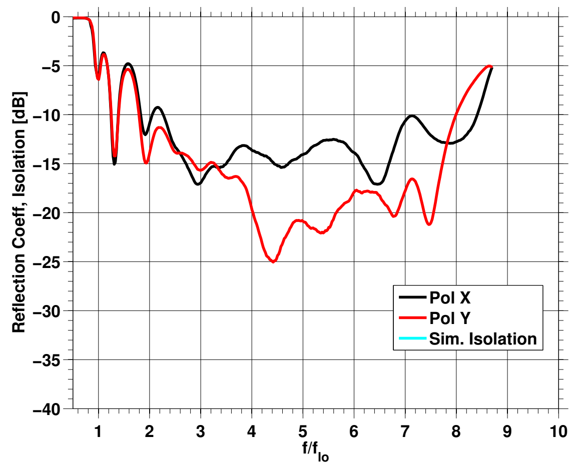

Figure 4.34: Measured scattering parameters of the very low gain QRFH

The patterns of this horn are measured and are presented in polar format in Figure 4.35. However, the measurements were incorrectly performed with the two antennas in the near-fields of each other. This invalidates the phase measurements, but its impact on magnitude measurements is thought to be less pronounced. Further, high-frequency harmonics at the output of wideband amplifiers in the pattern measurement setup due to very strong low-frequency RFI have plagued these measurements. Nevertheless, the measurements are presented here along with the simulated three-dimensional patterns in Figure 4.36.

Both the measured and the simulated far-fields underline the difficulty in designing such wide-beamwidth quad-ridge horns. Beamwidth control becomes more difficult and unlike higher gain designs, there is a serious trade-off between low-frequency input match and high-frequency radiation pattern performance. This is in line with the discussion in Section 3.5 where it is stated that for a given aperture size, wider beamwidths require many more modes. Generating and controlling these become very challenging over such large bandwidths. The intensity plots of E_x also show that near operating frequency of f_{lo}, the horn is too small and there is much energy "leaking" outside the aperture towards the back and sides.

4.6.3 Predicted system performance

Just as is done for the other quad-ridge horns presented herein, aperture efficiency of the Westford radio telescope when illuminated by the very low gain QRFH is calculated using physical optics and losses due to blockage, struts, surface errors are neglected. Because the primary mirror is a symmetric paraboloid, the physical optics calculations reduce to that of an 18.3 meter parabola with the QRFH at prime focus.

Figure 4.38 presents the predicted efficiency using both the simulated and measured patterns. The efficiency using measured patterns falls rapidly with frequency which is completely due to the

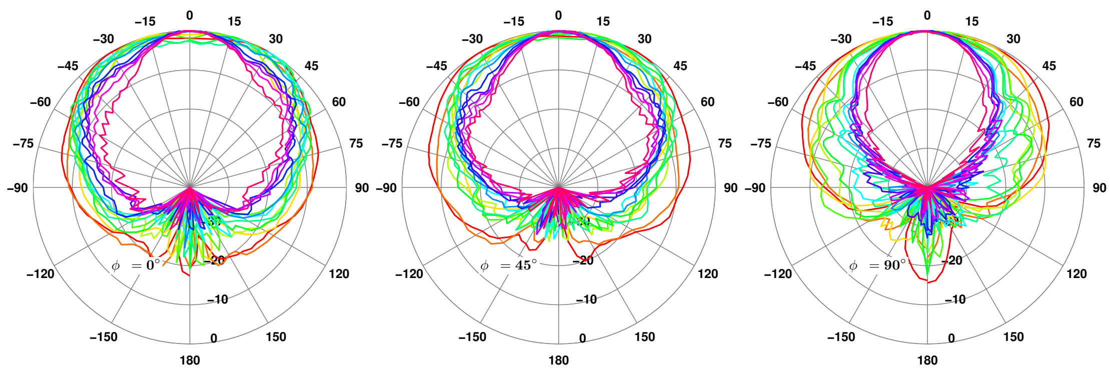

(a)

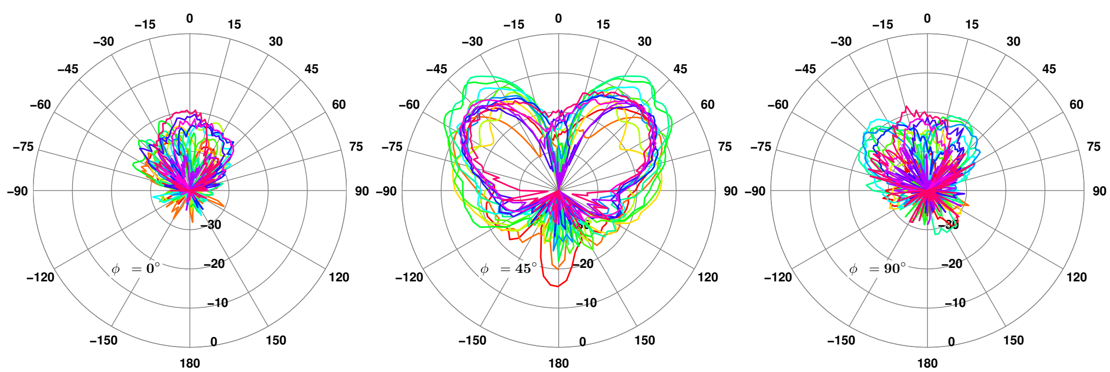

(b)

(c)

Figure 4.35: Measured (a) co-polarized, (b) cross-polarized (Ludwig 3rd definition) radiation patterns of the very low gain QRFH in $\phi = 0°$, $45°$, $90°$ azimuthal planes over the frequency range $f/f_{lo} = [1, 6]$. Part (c) shows photo of the horn during pattern measurements where the two antennas were incorrectly placed in each other's near-field regions.

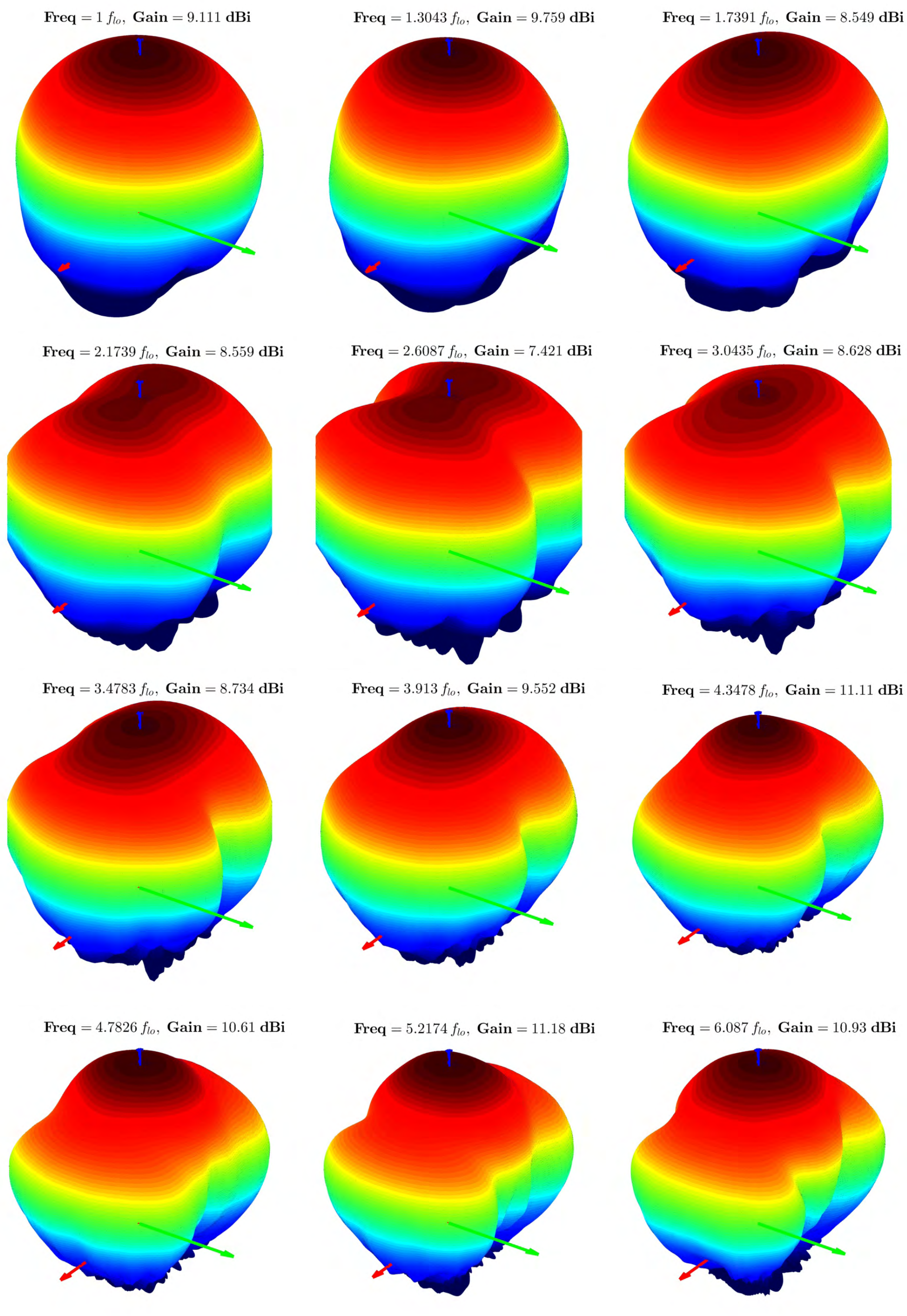

Figure 4.36: Three-dimensional simulated far-field patterns of the very low gain QRFH

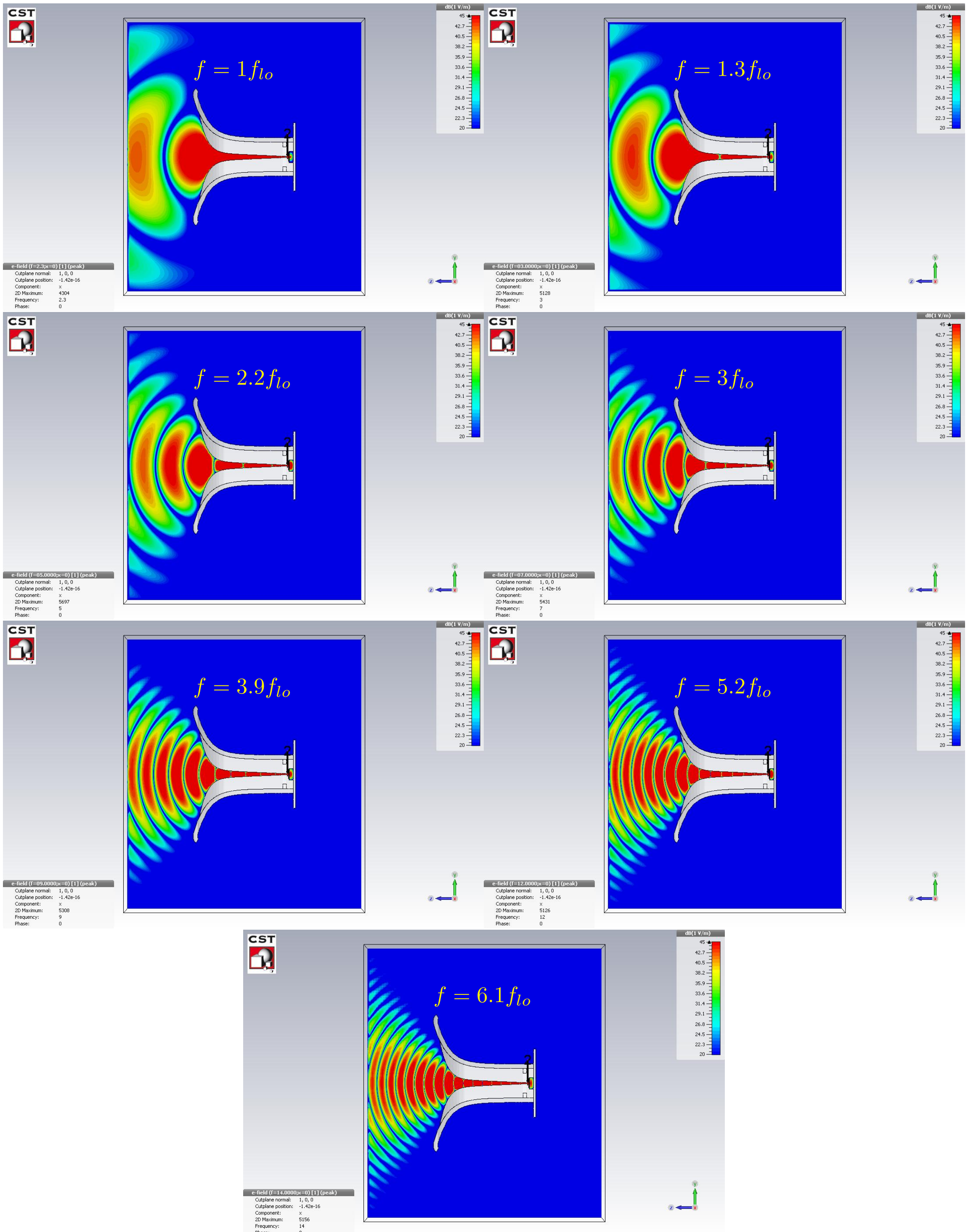

Figure 4.37: Intensity plots of E_x on the $x = 0$ plane in the very low gain quad-ridge horn which is excited in the x-polarization

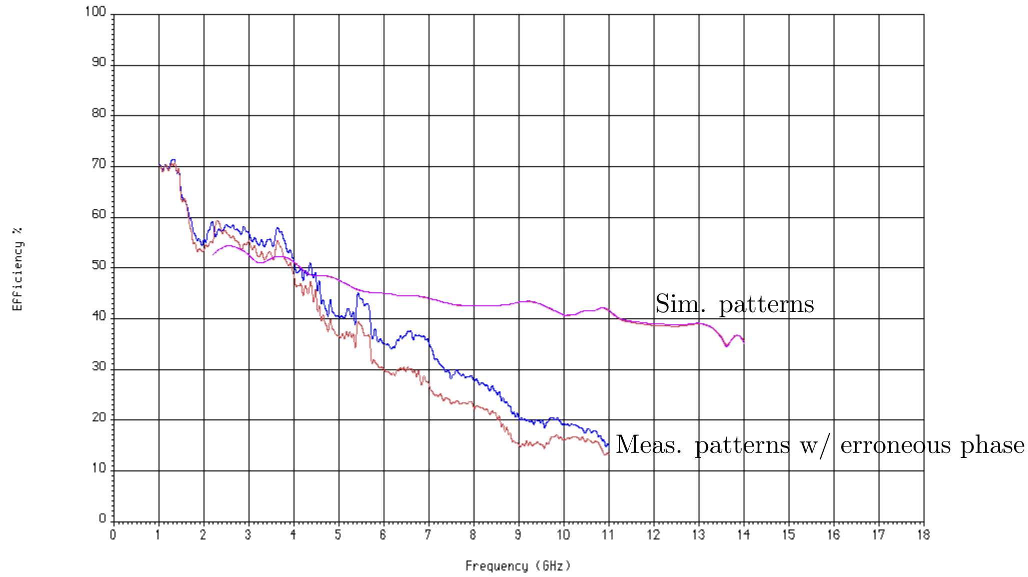

Figure 4.38: Predicted aperture efficiency of an 18.3 meter prime-focus telescope with f/D =0.3 with the very low gain QRFH as the feed antenna. The efficiencies using both simulated and measured patterns are plotted where the latter is significantly lower due to phase error in measurements. The efficiencies are calculated using physical optics and losses due to RMS surface error, blockage, struts, etc., are ignored. Telescope is assumed to point near zenith for noise temperature calculations.

aforementioned error in pattern measurements resulting in erroneous phase data. This was verified by computing the efficiency using the combination of measured far-field magnitude and simulated far-field phase (not shown for clarity) which yielded results very similar to the efficiency using simulated patterns only.

The predicted aperture efficiency is the lowest among all the quad-ridge horns presented, > 40 % over much of the frequency range of interest 2.3 to 14 GHz but falling as low as 35% above 13.5 GHz. A circular quad-ridge horn covering 0.6–2.5 GHz with approximately the same beamwidth as this one was also designed at Caltech and built in Germany by the Max Planck Institute for Radio Astronomy. It also achieves 40–45% aperture efficiency, according to simulations, at prime focus on the Effelsberg telescope [64].

4.7 Conclusions

Simulated and, where available, measured performance—both stand-alone and on-telescope—of five QRFH designs with nominal 10 dB beamwidths from 30 to 140 degrees have been presented. These results highlight the most appealing aspects of the horn:

1. Good beamwidth stability in E- and D- planes over 6:1 frequency range;
2. Ability to design the horn with nominal 10 dB beamwidths from 30 to 140 degrees;
3. Excellent single-ended match to 50 Ohm nominal impedance;
4. Ability to easily scale the horn for different frequency ranges;

while also bringing out some aspects that need further improvement (especially for large beamwidth horns):

1. Poor beamwidth stability in H-plane
2. Maintaining good radiation pattern performance for designs with beamwidths $>$ 110-120 degrees;
3. $>$ -10 dB peak cross-polarization in the D-plane over narrow frequency ranges.

Improving these aspects of the horn necessitates a thorough understanding of mode coupling and progression within the quad-ridge horn which is a topic of ongoing research. The aperture mode coefficients of the three of the five horns were also presented.